



# Identification of most spectrally distinguishable phenological stage of invasive *Phragmites australis* in Lake Erie wetlands (Canada) for accurate mapping using multispectral satellite imagery

Prabha Amali Rupasinghe · Patricia Chow-Fraser

Received: 21 July 2018 / Accepted: 20 June 2019 / Published online: 27 June 2019  
© Springer Nature B.V. 2019

**Abstract** *Phragmites australis* (Cav.) Trin. ex Steudel subspecies *australis* is one of the worst plant invaders in wetlands of North America. Remote sensing is the most cost-effective method to track its spread given its widespread distribution and rapid colonization rate. We hypothesize that the morphological and/or physiological features associated with different phenological states of *Phragmites* can influence their reflectance signal and thus affect mapping accuracies. We tested this hypothesis by comparing classification accuracies of cloud-free images acquired by Landsat 7, Landsat 8, and Sentinel 2 at roughly monthly intervals over a calendar year for two wetlands in southern Ontario. We used the Support Vector Machines classification and employed field observations and image acquired from unmanned aerial vehicle (8 cm) to perform accuracy assessments. The highest *Phragmites* producer's, user's, and overall accuracy (96.00, 91.11, and 88.56% respectively) were provided by images acquired in late summer and fall period. During this period, green, Near Infrared, and Short-Wave Infrared bands generated more unique reflectance signals for *Phragmites*. Both Normalized Difference Vegetation Index and Normalized Difference Water Index showed significant difference between *Phragmites* and the most

confused classes (cattail; *Typha latifolia* L., and meadow marsh) during the late summer and fall period. Since meadow marsh separated out best from *Phragmites* and cattail in the February image, we used it to mask the meadow marsh in the July image to reduce confusion. The unique reflectance signal of *Phragmites* in late summer and fall is likely due to prolonged greenness of *Phragmites* when compared to other wetland vegetation, large, distinct inflorescence, and the water content of *Phragmites* during this period.

**Keywords** *Phragmites* · Wetlands · Multispectral images · SVM classification

## Introduction

*Phragmites australis* subsp. *Australis* (Cav.) Trin. ex Steudel (the common reed) is a perennial grass that grows in aquatic, semi-aquatic, and terrestrial habitats throughout the world. Saltonstall (2002) identified 27 genetically distinct groups (haplotypes) worldwide, of which 11 have been found in North America. Over the past two decades, the European haplotype M began to make rapid incursions into Canada and the U.S., especially into coastal wetlands of the Laurentian Great Lakes (Wilcox et al. 2003; Tulbure et al. 2007; Wilcox 2012; Bourgeau-Chavez et al. 2015), and

P. A. Rupasinghe (✉) · P. Chow-Fraser  
Department of Biology, McMaster University, 1280 Main  
St. West, Hamilton, ON L8S 4K1, Canada  
e-mail: rupasingp@mcmaster.ca

along highway corridors (Saltonstall 2002; Lelong et al. 2007). This haplotype exhibits invasive characteristics, including its ability to aggressively colonize exposed mud flats sexually (through seeds), and then expand asexually (through rhizomes) to form dense monocultures that inhibit biodiversity of other plants and wildlife (Meyerson et al. 2000; Markle and Chow-Fraser 2018). Its rapid spread has been attributed to it being a superior competitor against other emergent vegetation (Rickey and Anderson 2004; Uddin et al. 2014) and to being more tolerant of disturbances (e.g. road maintenance and changes in hydrologic regimes) and stress (e.g. increased salinity due to road de-icing salts) (McNabb and Batterson 1991; Marks et al. 1994; Chambers et al. 1999; Saltonstall 2002).

Due to its competitive traits against native wetland vegetation, the invasive haplotype (henceforth referred to as invasive *Phragmites*) has successfully invaded many wetlands in south western Ontario and have become the dominant species since the late 1990s. Despite the destructive nature of this invader, very little control of invasive *Phragmites* occurred in the province of Ontario until a pilot project in 2007 involving Roundup Ultrá (Gilbert 2015). Glyphosate, the active compound in Roundup Ultra2 had already been found to be effective in controlling the growth of invasive *Phragmites* in several jurisdictions within the USA (Gilbert 2015). Other than chemical control, mechanical control and prescribed burning is also being used currently for *Phragmites* management. To track the rapid rate of colonization and to assess the effectiveness of control strategies implemented, frequent monitoring and mapping of wetland vegetation has become an essential aspect of sustainable marsh management (Adam et al. 2010).

Traditional floristic mapping requires extensive field work, collection of taxonomic information, ancillary data analysis, and visual estimation of percentage cover of each species, which are costly and labor intensive (Lyon and McCarthy 1995). Due to these limitations, traditional mapping programs have been limited to studies at the site level. For mapping wetland at the regional level, more cost-effective remote sensing techniques can be used because they require comparatively less but more strategic field surveys, and less time required for mapping protocols. An additional benefit is that remotely sensed imagery is acquired repeatedly and provide archived data, which can be easily incorporated into a Geographic

Information System (GIS) for further analyses and to study the spatial dynamics of plant assemblages (Ozesmi and Bauer 2002). Such approaches have been used successfully to map invasive plant species in marshes, where the absence of tree cover gives the sensor an unblocked view of the target species (Laba et al. 2008; Hestir et al. 2008; Bourgeau-Chavez et al. 2015).

Mapping individual species in marshes have several challenges. First, meteorological conditions can lead to lower accuracy because the specular reflectance of sunlight by the water surface often mixes with the signature of other land-cover classes (Bostater et al. 2004; Morel and Bélanger 2006). Water depth, presence of suspended and dissolved materials in the water column, and flow conditions can also affect reflectance by water, which would eventually affect land-cover classification (Hestir et al. 2008). Previous researchers have dealt with these water-related challenges by using different empirical criteria, image correction with field spectrometer measurements, and adjusting image acquisition time in case of air borne data (Bostater et al. 2004; Morel and Bélanger 2006). Other than the physical conditions, biological heterogeneity may also affect mapping accuracy of wetland vegetation.

Differences in phenological stage (i.e. timing of flowering, senescence, and changes in leaf and canopy structure) can also influence the reflectance signatures of co-occurring species (Hestir et al. 2008). Since most of the wetland species share similar habitats and are adapted to the same environmental conditions, they share similar morphological features such as leaf arrangement and canopy architecture that are difficult to distinguish visually. By identifying the phenological stages of the target species that help them stand out from co-occurring species, however, it should be possible to improve mapping accuracy. According to Zhang et al. (2003), four transition dates define the key phenological phases of a species: (1) green-up (date of onset of photosynthetic activity), (2) maturity (date when green leaf area is maximum), (3) senescence (rate at which greenness decreases), and (4) dormancy (date at which photosynthetic rate approaches zero). At regional and larger scales, variations in the composition of the community, micro- and regional climate regimes, soils, land management and plant-related features can lead to multiple modes of growth and senescence within a single annual cycle (Zhang

et al. 2003). Therefore, use of appropriate type of remotely sensed imagery collected in the most spectrally distinguishable phenological state, data pre- and post-processing techniques, and the classification algorithms may all affect the outcome.

Successful mapping of wetlands at the species level has typically required data with high spatial and spectral resolution (Everitt et al. 1995, 1996, 2001; Fuller 2005). Some sensors that have been used previously used include airborne hyperspectral sensors such as AVIRIS (Airborne Visible InfraRed Imaging Spectrometer; 224 bands) (Williams and Hunt Jr 2002), CASI (Compact Airborne Spectrographic Imager; 288 bands) (Schmidt and Skidmore 2001), HyMap (Hydrological Modeling and Analysis Platform; 126 bands) (Zhang and Xie 2013), and PROBE-1 (128 bands) (Lopez et al. 2004) and high resolution multispectral satellite imagery such as IKONOS (Fuller 2005; Sanchez-Flores et al. 2008) and QuickBird (Laba et al. 2008). Their relatively high cost and limited spatial cover (in the case of airborne data), however, make them unsuitable for frequent large-scale mapping that is required to track invasive *Phragmites* with high growth rates. By comparison, imagery with moderate spatial and spectral resolution (10 to 100 m spatial resolution and < 100 bands) have been commonly used for community-level mapping and have not been used for species-level mapping except when they occur as monocultures (Dewey et al. 1991; Sohn and McCoy 1997; Zhang et al. 2003). Some of the moderate-resolution data used for species identification include Landsat TM (Thematic Mapper; 7 bands) and ETM+ (Enhanced Thematic Mapper Plus; 8 bands) (Peterson 2005; Resasco et al. 2007; Huang and Asner 2009), SPOT (Satellite Pour l'Observation de la Terre; 4 bands) (Rasolofoharino et al. 1998), and ASTER (Advances in Spaceborne Thermal Emission and Reflection Radiometer; 14 bands) (Gao and Liu 2008) and MODIS (Moderate-resolution Imaging Spectroradiometer; 36 bands) (Zhang et al. 2003).

Despite its moderate spatial resolution (i.e. 30 m), Landsat data had been used by many researchers around the globe for species-level mapping. These images are particularly useful because the imagery are free, available every 16 days, provide extensive coverage, and date back to 1984 (Peterson 2005; Resasco et al. 2007). Moreover, Sentinel 2, a relatively new sensor (with 10, 20, and 60 m spatial resolution)

launched in 2015, has been used for the classification of crop and tree species, development of vegetation indices, Leaf Areas Index (LAI), and biophysical variables analysis etc. To date, however, it has not yet been used extensively in phenological studies (Delegido et al. 2011; Frampton et al. 2013; Hill 2013; Immitzer et al. 2016).

Besides selection of data, classification accuracy will depend on proper selection of the classification algorithm. Support Vector Machines (SVM) classification is a supervised, non-parametric, statistical learning technique developed by Vapnik in 1979 (Vapnik and Kotz 1982). As this method does not assume data normality distribution, it usually performs better than many popular classifiers such as the maximum likelihood classification (Dalponte et al. 2008; Rupasinghe et al. 2018). The SVM performs better in terms of classification accuracy, computational time, and stability to parameter setting when compared with radial basis function neural networks and K-nearest neighbor classification methods (Melgani and Bruzzone 2004; Pal and Mather 2005). Moreover, this method can produce high classification accuracy using a relatively small training data set (Dalponte et al. 2008; Zheng et al. 2015). Consequently, over the past decade, SVM classification has gained popularity in the remote sensing community (Mountrakis et al. 2011). Many past investigators have successfully used the SVM classification in forest and crop classification, species-level mapping in wetlands, and in developing vegetation indices for different data sources such as hyperspectral (Gualtieri and Crompt 1999), LiDAR (Dalponte et al. 2008), and multispectral data including Landsat TM (Huang et al. 2008; Zheng et al. 2015) and Sentinel 2 (Stratoulis et al. 2015).

Previous studies have demonstrated that the moderate resolution multispectral images could be used to map invasive species that form large monocultures however, the reflectance signal of these invasive species are often very similar to the native species that share the same ecosystem. This may lead to low classification accuracy for both invasive and native species. Therefore, it is important to identify the vegetation categories that have similar reflectance signatures as the invasive species to develop more accurate classification protocols. Moreover, the effect of biological heterogeneity highly varies depending on the site conditions and the species composition of the

study area. In this study, we address these issues and focus mainly on the effect of different phenological states on mapping accuracy of selected Lake Erie wetlands, with special emphasis on invasive *Phragmites*. We evaluated the use of SVM classification to map large monocultures of *Phragmites* in two Lake Erie wetlands using Landsat 7, 8, and Sentinel 2 imagery. To minimize omission errors associated with classification of mixed pixels (*Phragmites* and similar land cover classes) when moderate resolution imagery are used for species level classification, and as limited spectral bands are available in multispectral imagery, we have analyzed the time series images collected over different months of the calendar year to determine the best time in the *Phragmites* growth cycle or the best phenological state when the plant will produce a reflectance signature that will be most unique when compared with co-occurring vegetation. For future applications with other image sources, we have also identified the bands that contributed most to distinguishing among *Phragmites* and other similar vegetation classes. In summary, this novel *Phragmites* mapping approach; 1. Will provide cost-effective method to identify *Phragmites* invaded wetlands using freely available, moderate-resolution satellite images for large-scale monitoring and treatment effectiveness monitoring programs, 2. Will provide the wetland management community with an accurate, cost-effective method to track changes in the distribution of invasive *Phragmites* at a regional scale, and 3. Support future research to accurately map *Phragmites* with other sensors which provide important spectral information and to collect images during the best period of the year and plan field work accordingly.

## Methods

### Study sites

We conducted the study in two Lake Erie wetlands, Big Creek National Wild Life Area (BCNWA) (49°59'N 80°46'W) and Rondeau Bay Marsh (RBM) (42°17'N 81°52'W) (Fig. 1). BCNWA is located on the North shore of Lake Erie, 3 km from the southwest Port Rowan and at the head of the Long Point Bay on Lake Erie, in the Regional Municipality of Haldimand-Norfolk county (Ashley and Robinson 1996; Environment and Climate Change Canada 2011). It is

a 771-ha complex consisting of two sub-units, Big Creek unit (615 ha) and the Hahn Marsh Unit (156 ha). Our study focused on the Big Creek unit, which is managed by the Environment and Climate Change Canada. Wetlands at this site is dominated by Blue-joint Grass (*Calamagrostis canadensis* (Michx.) P. Beauv.), cattails (*Typha latifolia* L.), and sedges (Ashley and Robinson 1996). The invasive species in this site includes *Phragmites*, European frog-bit (*Hydrocharis morsus-ranae* L.) and European Black Alder (*Alnus glutinosa* (L.) Gaertn.) (Environment and Climate Change Canada 2011).

RBM is a shallow coastal wetland, also on the northern shore of the central basin of the Lake Erie, approximately 100 km southeast of Windsor ON, Canada and Detroit, MI, USA (Meloche and Murphy 2006; Glass et al. 2012). It was established in 1894 and was Ontario's second protected provincial park. It covers an area of 3257 ha and mainly consists of forests, sandy peninsula, and marsh. Forested land in RBM is characterized by rare Carolinian tree species, where it is the largest remaining representation of Carolinian forests in Canada and is a primeval or wilderness remnant of the vegetation of early Ontario (Mann and Nelson 1980; McLaughlin 1993). Approximately 40% of the rare, threatened or endangered species in Canada are Carolinian and are present in RBM.

We used the BCNWA site for development of our classification protocols as this site had not been treated during the study period and there were no significant changes in *Phragmites* cover over the period studied. We used the RBM site for comparison of results obtained from the BCNWA site to evaluate the validity of our methods. We did not use this site for initial methods evaluation because the site had been treated for invasive *Phragmites* during the study period, and this limited the amount of time when our ground reference data were valid.

### Ground reference data

As the ground reference for BCNWA, we used manually digitized land-cover maps that were created with field data collected from two previous studies (Marcaccio et al. 2016; Markle and Chow-Fraser 2018). One study was focused on habitat use by Blanding's turtles (*Emys blandingii* (Holbrook, 1838)) and included vegetation surveys conducted between

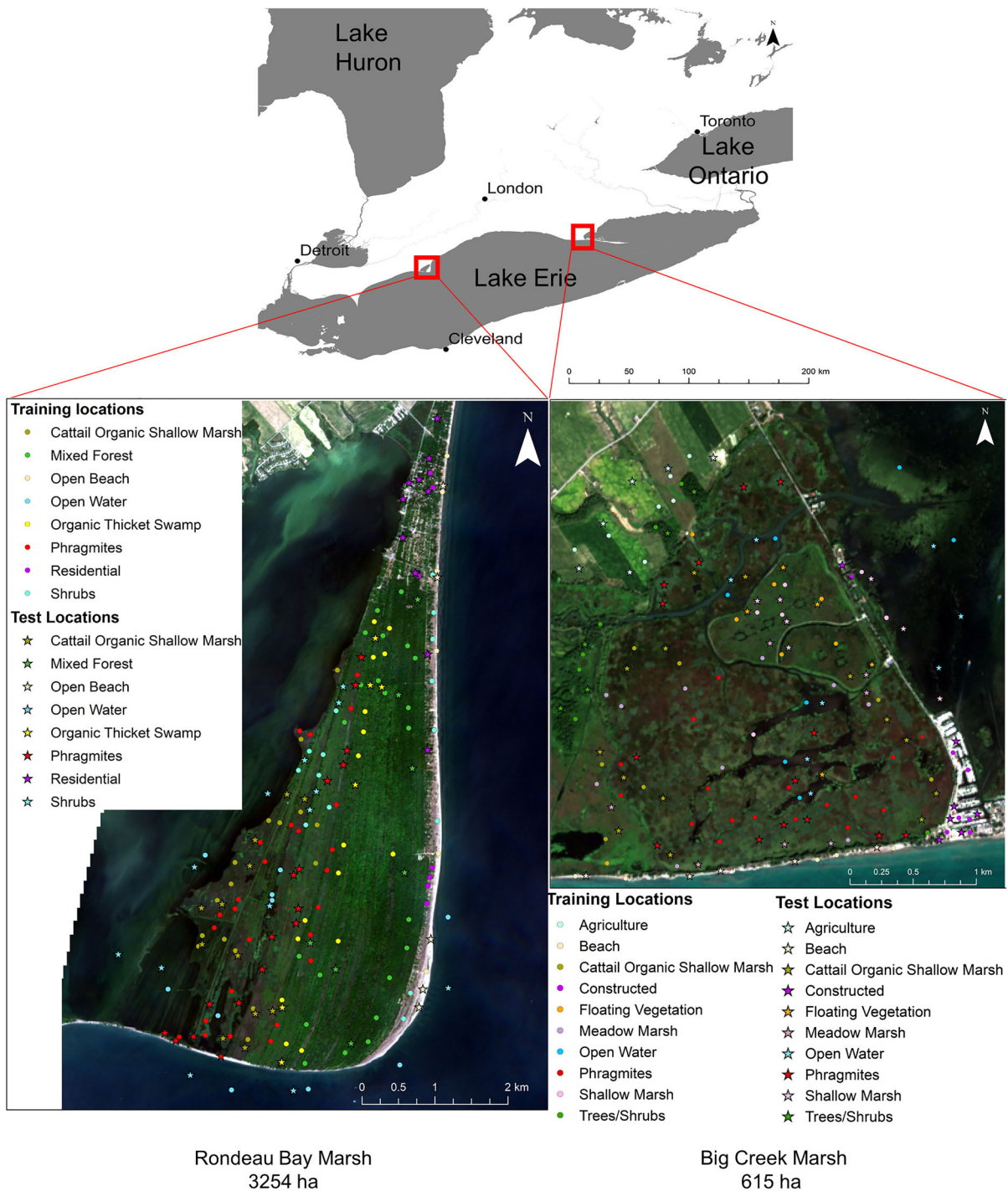


**Fig. 1** Location of study sites and test and training locations used for classification

14 July and 14 August 2014. In this study, 176 quadrats (2 m × 2 m) were used to identify the vegetation data (Markle and Chow-Fraser 2018),

which included aquatic marsh, cattail marsh, meadow marsh, mixed organic marsh, open water, invasive *Phragmites*, treated invasive *Phragmites*, upland, and

other land-cover types (e.g.: swamp, thicket). Marcaccio et al. (2016) have created vegetation maps using imagery collected with a fixed-wing unmanned aerial vehicle (UAV; Sensefly eBee Canon ELPH 110 HS, 4 cm spatial resolution for red, green and blue bands) on 4 September 2015 during clear-sky conditions based on the field surveys conducted by Markle and Chow-Fraser (2018).

As ground reference for the RBM site, we used manually digitized orthophotos (South Western Ontario Orthophotography Project; SWOOP; 20 cm spatial resolution for red, green and blue bands) collected in 2010 and 2015 that has been used in same study by Markle and Chow-Fraser (2018). Field data from a vegetation survey conducted in summer 2011 and 2013 were used to create manually digitized maps for 20 land cover classes, including bulrush organic shallow marsh, campground, cattail organic shallow marsh, fen, floating leaved shallow marsh, meadow marsh, mixed forest, mixed shallow aquatic marsh, mixed woodlands, open beach, open field, open water, organic thicket swamp, invasive *Phragmites*, residential, road, rolled invasive *Phragmites*, shrub beach, shrubs, and trail. (Markle and Chow-Fraser 2018). Other than the field data, we also used locations of where invasive *Phragmites* had been treated between 2009 and 2014 (Gibert 2015) as ground reference.

For the current study, we used eleven land cover classes for the BCNWA (Agriculture, beach, cattail organic shallow marsh, constructed, floating vegetation, meadow marsh, open water, *Phragmites*, shallow marsh, and trees/shrubs) and eight classes for RBM (cattail organic shallow marsh, mixed forest, open beach, open water, organic thicket swamp, *Phragmites*, residential, and shrub beach).

#### Image data

Multispectral satellite data from Landsat 7, Landsat 8 and Sentinel 2 were used in this study (Table 1). Landsat is the longest continuous record of satellite observations owned by United States Geological Survey (USGS) and National Aeronautics and Space Administration (NASA). The Landsat mission consists of eight satellites, and currently both Landsat 7 and 8 are active. Landsat 7 was launched in 1999 and Landsat 8 was launched in 2013. Sentinel 2 is a satellite owned by the European Space Agency (ESA), designed for studies based on terrestrial observations.

It consists of two satellites, Sentinel-2A (launched in 2015) and Sentinel-2B (launched in 2017).

We downloaded all cloud-free images corresponding to the year when respective vegetation surveys had been conducted; when no cloud-free images for particular months were available that year, we sought image data acquired immediately prior to or following the survey year. We assumed that the changes in cover of *Phragmites* between two consecutive years are relatively small. For the both BCNWA and RBM sites, we used a total of fourteen Landsat 7, fourteen Landsat 8, and twelve Sentinel 2 images. We used ENVI 5.5 (Harris Geospatial 2018) to radiometrically and atmospherically (ENVI FLAASH atmospheric correction) correct images to obtain the surface reflectance from the digital numbers. For the Sentinel 2 images, six bands which had 20-m spatial resolution (Table 1) were resampled to 10 m and pre-processed separately. We then stacked the resampled bands with 10 m bands for the post-processing. We used reflectance images for all image classifications.

#### Image classification and phenological analysis

We used SVM classification to classify the time-series reflectance images of Landsat 7 and 8 and Sentinel 2 for BCNWA site for selected bands (Table 1). Using ArcGIS 10.5, we first generated random points within the manually digitized land cover maps from UAV and orthophotos using the vegetation survey data for both study sites separately (ten points per land cover class, located at the center of the polygons to avoid mixed pixels at the edges; Fig. 1). We then used the random points to manually create Regions Of Interest (ROI) in ENVI 5.5, capturing 5 or more pixels per location (depending on the area occupied by the land-cover type under consideration) and used these as ground reference for image classification. We added more points for some classes during the classification process after evaluating the Jefferies-Matusita separability to increase the separability of classes with poor separability prior to the image classification. We conducted the image classification for both sites using the classes mentioned under the “Ground reference data”. For accuracy assessment, we used a separate set of non-overlapping random points to create a minimum of 10 ROI’s (Fig. 1), consisting of one to ten image pixels each, per vegetation class and information about the vegetation types collected in the field.

**Table 1** Comparison of spectral bands of Landsat7, Landsat 8 and Sentinel 2

| Spectral Band            | Landsat 7        |                        | Landsat 8          |                        | Sentinel 2      |                        |
|--------------------------|------------------|------------------------|--------------------|------------------------|-----------------|------------------------|
|                          | Wavelength (µm)  | Spatial resolution (m) | Wavelength (µm)    | Spatial resolution (m) | Wavelength (µm) | Spatial resolution (m) |
| Coastal aerosols         | –                | –                      | <b>0.433–0.453</b> | 30                     | 0.443           | 60                     |
| Blue                     | <b>0.45–0.52</b> | 30                     | <b>0.450–0.515</b> | 30                     | <b>0.490</b>    | 10                     |
| Green                    | <b>0.52–0.60</b> | 30                     | <b>0.525–0.600</b> | 30                     | <b>0.560</b>    | 10                     |
| Red                      | <b>0.63–0.69</b> | 30                     | <b>0.630–0.680</b> | 30                     | <b>0.665</b>    | 10                     |
| Vegetation Red Edge      | –                | –                      | –                  | –                      | <b>0.705</b>    | 20                     |
| Vegetation Red Edge      | –                | –                      | –                  | –                      | <b>0.740</b>    | 20                     |
| Vegetation Red Edge      | –                | –                      | –                  | –                      | <b>0.783</b>    | 20                     |
| NIR                      | <b>0.77–0.90</b> | 30                     | <b>0.845–0.885</b> | 30                     | <b>0.842</b>    | 10                     |
| Narrow NIR               | –                | –                      | –                  | –                      | <b>0.865</b>    | 20                     |
| Water vapor              | –                | –                      | –                  | –                      | 0.945           | 60                     |
| Cirrus                   | –                | –                      | 1.360–1.390        | 30                     | –               | –                      |
| SWIR-Cirrus              | –                | –                      | –                  | –                      | 1.375           | 60                     |
| SWIR1                    | <b>1.55–1.75</b> | 30                     | <b>1.560–1.660</b> | 30                     | <b>1.610</b>    | 20                     |
| SWIR2                    | <b>2.90–2.35</b> | 30                     | <b>2.100–2.300</b> | 30                     | <b>2.190</b>    | 20                     |
| Long Wavelength Infrared | –                | –                      | 10.30–11.30        | 100                    | –               | –                      |
| Thermal                  | 10.40–12.50      | 60*(30)                | –                  | –                      | –               | –                      |
| Long Wavelength Infrared | –                | –                      | 11.50–12.50        | 100                    | –               | –                      |
| Panchromatic             | 0.52–0.90        | 15                     | 0.500–0.680        | 15                     | –               | –                      |

*NIR* near infrared; *SWIR* short wave infrared (bands used in the study are in bold)

We identified the months with highest classification accuracy in terms of overall accuracy and *Phragmites* user's and producer's accuracy.

We used the same set of ROIs used for the classification to analyze the Jefferies-Matusita separability of *Phragmites* with the other land-cover classes for the time series images. Jefferies–Matusita separability is a quantitative evaluation of spectral separability and it indicates how well the selected ROI pairs are statistically separate for images collected in different phenological stages. Separability values were plotted with Microsoft Excel 2016. Based on the separability values, we identified classes that were most confused with *Phragmites*.

Furthermore, we stacked the Landsat 8 images collected in each season (March to June: spring, June to September: summer, September to December: Fall, and December to March: winter) and repeated the SVM classification using the bands from all the images per season combined as input. Here, we expect

to combine fine spectral changes of species throughout the season to improve the classification and to minimize the effect from the changing water levels through each season. We also performed a Principal Component Analysis (PCA) on the stacked images and repeated the classification on all PCA bands. We used Minitab 18 to perform a two-way ANOVA followed by Tukey's test to determine significant differences across seasons and across satellites after pooling the results from single months, seasons combined, and a PCA of the pooled data as there were no significant difference across the groupings.

To identify what plant feature, greenness or the plant water status (i.e. Plant function) is responsible for *Phragmites* mapping accuracy we calculated the Normalized Difference Vegetation index (NDVI) and Normalized Difference Water Index (NDWI) for monthly Landsat 8 images in the time series. Moreover, to identify which spectral bands contributed most to *Phragmites* separability, we evaluated the

reflectance changes of each band for Landsat 8 for the time series images. We generated 30 random points per vegetation class in ArcGIS (10.5), extracted the reflectance values for all the bands (Table 1), and calculated NDVI and NDWI per point. We calculated the mean values for reflectance, NDVI, and NDWI per vegetation class throughout the year, plotted the changes, and determined the time at which NDVI and NDWI were most different between *Phragmites* and the confused vegetation classes. We used One-way ANOVA and Tukey's test in Minitab 18 to identify significantly contributing bands and indices for *Phragmites* mapping accuracy. We also excluded one band at a time for Landsat 8 image that provided the highest classification accuracy and repeated the SVM classification to identify the bands that contributed most to the *Phragmites* spectral signature.

To compare the results from BCNWA site, we repeated the image classification, the separability analysis, and conducted the analysis to determine the bands that contributed most to the indices in the RBM site. We did not perform the multi-temporal image classification for this site as RBM had been treated for invasive *Phragmites* during the study period. A summary of the methods used in this study is documented in Fig. 2.

#### Reduction of mapping confusion between *Phragmites* and meadow marsh mapping

Based on results from the “[Image classification and phenological analysis](#)”, we identified that the meadow marsh was the most confused class with *Phragmites* and that the highest separability between classes occurred in February. We also found the highest accuracy for *Phragmites* and other land-cover classes to be in July. Therefore, we created a mask for meadow marsh based on the Landsat 8 images acquired in February, applied the mask to the July images and repeated the SVM classification without the meadow marsh ROIs. For this image classification, we used the bands listed in Table 1. We used the same ground reference information, and protocols for image classification and accuracy assessment as described under “[Image classification and phenological analysis](#)”. We have also calculated the overlap area between *Phragmites* and meadow marsh with comparison to manually digitized vegetation maps for February,

July, and February-July combined maps using ArcGIS.

## Results

### Image classification and phenological analysis

The overall accuracy was highest in late summer and early fall (July to October), tapering at both ends of the calendar year. We observed similar trends for all three sensors examined (Tables 2, 3, 4 and Fig. 3). Both the user's and producer's accuracies of *Phragmites* followed the same trend, peaking in late summer and early fall. When the three sensors were compared, Sentinel 2 provided the highest *Phragmites* user's and producer's accuracy, while Landsat 8 provided the highest overall accuracy and Landsat 7 provided the lowest accuracy in all cases. The classification for BCNWA resulted in higher accuracy for both Landsat 8 and Sentinel 2. When these results were compared with those for the RBM site, we observed a similar trend in classification accuracy with respect to the three sensors but a higher accuracy for Landsat 7.

The most confused classes with invasive *Phragmites* were meadow marsh and the cattail organic shallow marsh. Separability of *Phragmites* with all other landcover classes were greatest in July, except when it was compared with meadow marsh; for the meadow marsh, the highest separability with the two other classes was observed in February (Fig. 4). As demonstrated in the error matrices, most of the commission error for *Phragmites* was attributed to confusion with cattail and meadow marsh (Tables 5, 6, 7). Other than for *Phragmites*, we also observed some confusion between agricultural lands and trees/shrubs, cattail and meadow marsh, and open water and shallow marsh (Tables 5, 6, 7). When compared with the RBM site, cattail organic shallow marsh was the most confused class with *Phragmites*. We excluded meadow marsh from the RBM site because meadow marsh occupied very little area and Landsat and Sentinel 2 spatial resolution did not capture this class accurately.

Classification of single images (single month) did not produce accuracies that differed significantly from classification of multiple images from different months that were combined into a single image (combined seasonal) or classification of pooled images

**Fig. 2** Flow chart of the methods used in the study

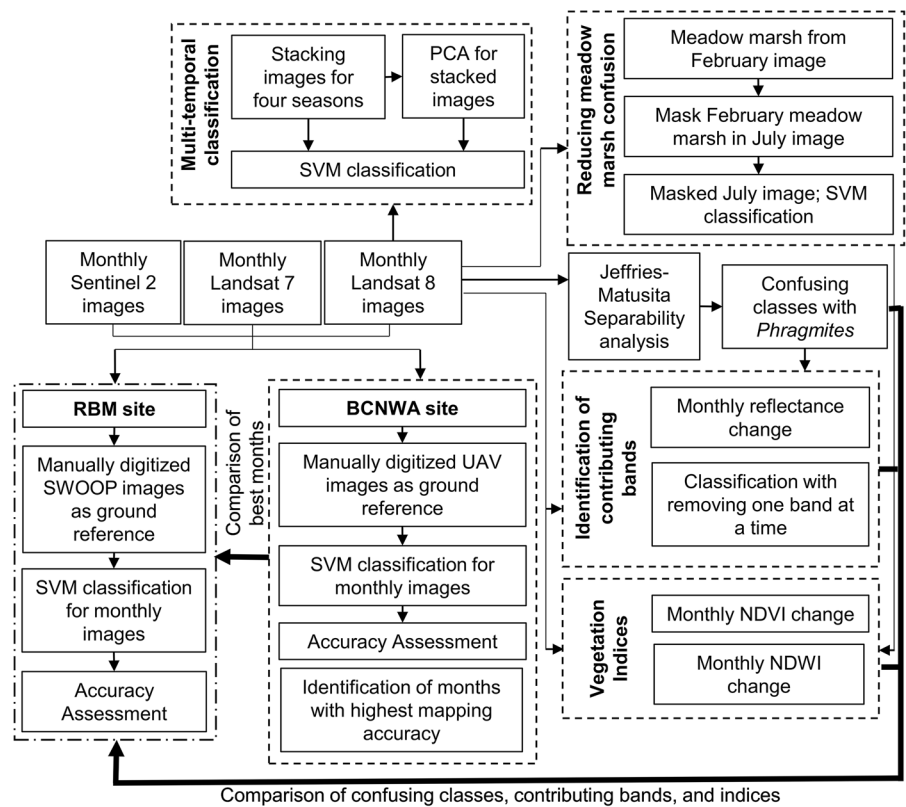


**Table 2** Monthly changes in mapping accuracy (%) for the two study sites using Landsat 7

| Big Creek   |              |              |              | Average      | Rondeau Bay |              |              |              | Average      |
|-------------|--------------|--------------|--------------|--------------|-------------|--------------|--------------|--------------|--------------|
| Date        | Producer's   | User's       | Overall      |              | Date        | Producer's   | User's       | Overall      |              |
| 2014 Feb 15 | 58.00        | 63.04        | 62.93        | 61.32        | 2009 Mar 13 | 60.00        | 79.00        | 80.21        | 73.07        |
| 2015 Mar 23 | 88.00        | 42.31        | 62.59        | 64.30        | 2010 May 03 | 70.00        | 80.00        | 83.03        | 77.687       |
| 2014 Apr 24 | 84.00        | 37.50        | 64.99        | 62.16        | 2011 Jun 07 | 53.33        | 72.73        | 80.26        | 68.77        |
| 2015 Jul 13 | 66.00        | 44.00        | 73.86        | 61.29        | 2010 Jul 06 | <b>90.00</b> | <b>81.82</b> | <b>85.96</b> | <b>85.93</b> |
| 2015 Jul 29 | <b>82.00</b> | <b>52.56</b> | <b>76.43</b> | <b>70.33</b> | 2009 Aug 04 | <b>76.67</b> | <b>79.31</b> | <b>81.14</b> | <b>79.04</b> |
| 2014 Aug 21 | <b>84.00</b> | <b>53.41</b> | <b>74.82</b> | <b>70.74</b> | 2010 Nov 11 | 53.33        | 76.19        | 79.83        | 69.78        |
| 2015 Sep 15 | <b>78.00</b> | <b>62.03</b> | <b>72.69</b> | <b>70.90</b> |             |              |              |              |              |
| 2015 Nov 02 | 74.33        | 66.67        | 62.49        | 67.83        |             |              |              |              |              |

Producer's and User's accuracy pertain to invasive *Phragmites*. Overall accuracy pertains to all classified classes

The months with highest overall accuracies are bolded

after a PCA was run (PCA seasonal; Fig. 5). We did not observe a significant difference with respect to overall or *Phragmites* user's and producer's accuracies among the single month, combined seasonal or PCA seasonal treatments. Therefore, we pooled the data for three groupings and conducted statistical analysis to

identify the seasons with highest classification accuracies. Our results indicated that summer and fall had homogeneous means when compared to the spring and winter. When considering the sensors, Sentinel 2 had the highest accuracy while Landsat 7 had lowest for overall and *Phragmites* user's accuracy. There were,

**Table 3** Monthly changes in mapping accuracy (%) for the two study sites using Landsat 8

| Big Creek   |              |              |              | Average      | Rondeau Bay |              |              |              | Average      |
|-------------|--------------|--------------|--------------|--------------|-------------|--------------|--------------|--------------|--------------|
| Date        | Producer's   | User's       | Overall      |              | Date        | Producer's   | User's       | Overall      |              |
| 2015 Feb 27 | 76.00        | 90.48        | 66.13        | 77.54        | 2014 Jan 14 | 81.25        | 70.27        | 65.78        | 72.43        |
| 2014 May 31 | 84.00        | 52.81        | 74.60        | 70.47        | 2014 Feb 15 | 84.38        | 58.70        | 63.12        | 68.73        |
| 2014 Jun 03 | 86.00        | 51.19        | 74.83        | 70.67        | 2014 Mar 03 | 68.75        | 59.46        | 65.40        | 64.54        |
| 2015 Jul 21 | <b>96.00</b> | <b>88.89</b> | <b>88.56</b> | <b>91.15</b> | 2014 Jun 04 | 53.13        | 54.84        | 71.48        | 59.82        |
| 2014 Aug 19 | <b>92.00</b> | <b>79.31</b> | <b>79.63</b> | <b>83.65</b> | 2014 Aug 10 | <b>79.59</b> | <b>73.58</b> | <b>75.00</b> | <b>76.06</b> |
| 2014 Sep 04 | <b>93.55</b> | <b>72.73</b> | <b>78.94</b> | <b>81.74</b> | 2014 Sep 27 | 81.25        | 48.15        | 67.68        | 65.69        |
| 2014 Nov 20 | 94.00        | 54.65        | 76.43        | 75.03        | 2014 Oct 10 | 71.00        | 61.54        | 71.62        | 68.05        |

Producer's and User's accuracy pertain to invasive *Phragmites*. Overall accuracy pertains to all classified classes

The months with highest overall accuracies are bolded

**Table 4** Monthly changes in mapping accuracy (%) for the two study sites using Sentinel 2

| Big Creek   |              |              |              | Average      | Rondeau Bay |              |              |              | Average      |
|-------------|--------------|--------------|--------------|--------------|-------------|--------------|--------------|--------------|--------------|
| Date        | Producer's   | User's       | Overall      |              | Date        | Producer's   | User's       | Overall      |              |
| 2016 Apr 27 | 87.69        | 63.10        | 81.71        | 77.50        | 2016 Apr 27 | 77.10        | 62.43        | 69.89        | 69.81        |
| 2016 May 28 | 62.56        | 40.53        | 73.23        | 58.77        | 2016 May 28 | 84.55        | 55.03        | 72.89        | 70.82        |
| 2016 Jul 06 | 93.85        | 84.33        | 82.82        | 87.00        | 2016 Jun 29 | 80.56        | 56.68        | 74.61        | 70.62        |
| 2016 Jul 27 | <b>95.35</b> | <b>91.11</b> | <b>84.00</b> | <b>90.15</b> | 2016 Jul 06 | <b>82.66</b> | <b>77.61</b> | <b>79.65</b> | <b>79.97</b> |
| 2016 Sep 26 | <b>92.82</b> | <b>87.44</b> | <b>86.11</b> | <b>88.79</b> | 2016 Dec 10 | 72.98        | 60.74        | 72.83        | 68.85        |
| 2016 Oct 15 | <b>87.18</b> | <b>72.34</b> | <b>82.88</b> | <b>80.80</b> |             |              |              |              |              |
| 2016 Dec 10 | <b>89.23</b> | <b>79.82</b> | <b>85.94</b> | <b>85.00</b> |             |              |              |              |              |

Producer's and User's accuracy pertain to invasive *Phragmites*. Overall accuracy pertains to all classified classes

The months with highest overall accuracies are bolded

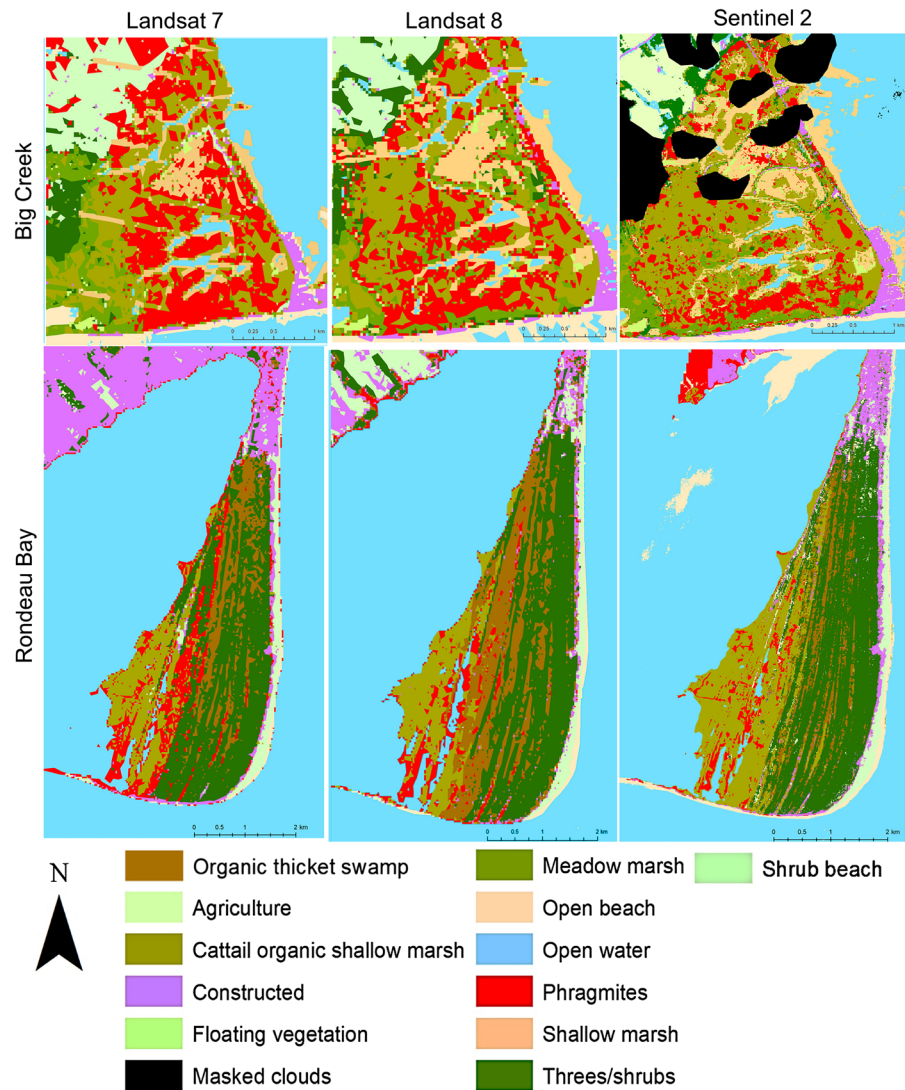
however, no significant differences in the *Phragmites* producer's accuracy between sensors (Fig. 6).

Since cattail and meadow marsh were most confused with *Phragmites*, we examined how respectively reflectance, NDVI and NDWI values changed over the time series for these three classes. Visually, coastal aerosols, blue, green, red, and SWIR2 (ShortWave InfraRed) bands associated with the three classes showed no difference in reflectance. The NIR (Near InfraRed) reflectance was higher for *Phragmites* than for cattail in July and August while reflectance for meadow marsh in February was greater than those for *Phragmites* and cattails. The SWIR1 reflectance for meadow marsh was slightly higher than that for *Phragmites* in August (Fig. 7). One-way ANOVA followed by Tukey's test shows that the greatest number of significant p-values were recorded for

green, NIR, and both SWIR bands when compared to the other bands. These results were consistent with the highest mapping accuracy of invasive *Phragmites* (i.e. the month associated with the greatest number of significant p-values) being recorded in July, August, and September in terms of separability between invasive *Phragmites* and cattail, whereas the highest mapping accuracy in regard to separability between invasive *Phragmites* and meadow marsh was recorded in February (Table 8).

Except for one band on a single occasion, accuracies associated with the image classification with excluding one band at a time provided a similar trend. Exclusion of green, NIR, and SWIR1 bands resulted in greater than 2% reduction in overall and *Phragmites* user's accuracies; however, *Phragmites* producer's accuracy remained constant through all bands and

**Fig. 3** Classified maps with SVM classification for Big Creek and Roundeau Bay, Lake Erie

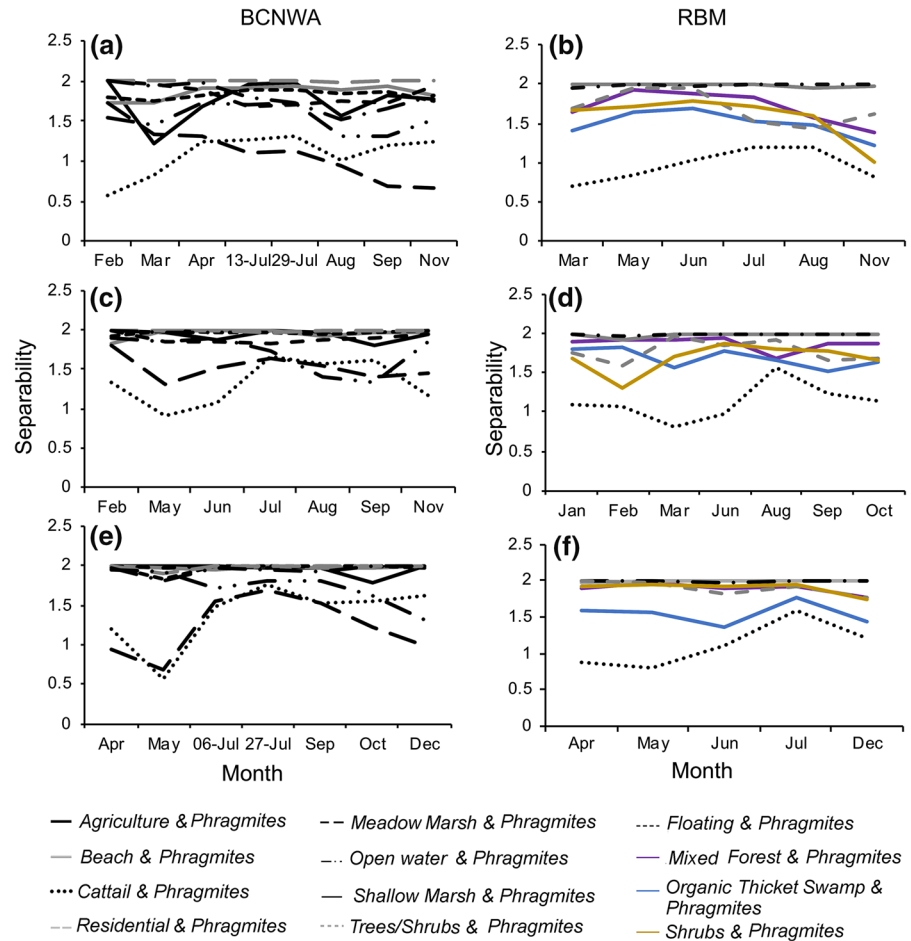


single-band exclusions (Table 9). Overall, these results suggest that the green, NIR, and SWIR reflectance of *Phragmites* contributed most to the unique reflectance signature that resulted in higher classification accuracy, especially with respect to cattail when compared to the other spectral bands. The results also confirmed that the highest *Phragmites* mapping accuracy could be obtained in the late summer and early fall period. When these results were compared with the RBM site, the green, NIR, and SWIR2 bands provided the greatest number of significant p-values. Images acquired in August also provided the most significant p-values. Results of image classification with band exclusions for the RBM

site did not show the same trend noted for the BCNWA site. There was more than 2% accuracy reduction for overall, *Phragmites* user's and producer's accuracy when the green band was excluded. Exclusion of NIR band only reduced *Phragmites* producer's accuracy while exclusion of SWIR2 band reduced both producer's and user's accuracy.

Next, we compared the NDVI and NDWI values of *Phragmites*, cattail and meadow marsh for the time series images (Fig. 8 and Table 10). The NDVI scores associated with August and September were significantly different from those of other months while NDWI scores associated with July, August and September were significantly different. The meadow

**Fig. 4** Monthly changes in Jeffries-Matusita Separability of *Phragmites* in Big Creek wetland for **a** Landsat 7, **c** Landsat 8 and **e** Sentinel 2 data; For RBM **b** Landsat 7, **d** Landsat 8 and **f** Sentinel 2 data



marsh class was significantly different from *Phragmites* with respect to NDVI and NDWI scores in the February image. These results suggested that both greenness and plant water use efficiency may affect the spectral signature of invasive *Phragmites*. There were no clear patterns associated with RBM for NDVI and NDWI scores, but we observed the most significant p-values in June, August, September, and October.

#### Reduction of mapping confusion between *Phragmites* and meadow marsh mapping

When classified images of February and July were compared visually, we observed a higher *Phragmites* commission error in July (11.11%), compared with that in February (9.52%; Fig. 9 and Table 3). There was also a 35 ha overlap between the mapped and actual meadow marsh in February compared with only

a 30 ha overlap in July. Furthermore, only 13 ha of meadow marsh was mapped as false *Phragmites* in February while 26 ha was mapped in July. When we combined the meadow marsh mapped in February with the July image, we found that the overall accuracy was reduced to 85.4% (kappa coefficient = 0.83) in the combined image; however, both *Phragmites* user's and producer's accuracies were increased to 92.3% and 96.0%, respectively. By combining images collected in these 2 months, the overlap between the mapped and actual meadow marsh was increased to 39 ha, while the commission error for meadow marsh was reduced to 15 ha.

#### Discussion

In this paper, we developed a novel approach to map *Phragmites* using freely available multispectral

**Table 5** Error matrix for Landsat 7 (2015 July 29) for the Big Creek (number of pixels)

| Classification results | Reference data |           |            |             |          |              |            |            |               |              |            | Total |
|------------------------|----------------|-----------|------------|-------------|----------|--------------|------------|------------|---------------|--------------|------------|-------|
|                        | Agriculture    | Beach     | Cattail    | Constructed | Floating | Meadow marsh | Open water | Phragmites | Shallow marsh | Trees/shrubs | Total      |       |
| Agriculture            | <b>67</b>      | 0         | 0          | 0           | 0        | 0            | 0          | 0          | 0             | 0            | 0          | 67    |
| Beach                  | 1              | <b>14</b> | 0          | 1           | 0        | 0            | 1          | 0          | 0             | 0            | 0          | 17    |
| Cattail                | 0              | 4         | <b>108</b> | 1           | 2        | 2            | 3          | 2          | 0             | 0            | 0          | 122   |
| Constructed            | 1              | 3         | 0          | <b>26</b>   | 0        | 0            | 0          | 0          | 0             | 0            | 0          | 30    |
| Floating               | 0              | 0         | 0          | 0           | <b>9</b> | 0            | 0          | 0          | 0             | 0            | 0          | 9     |
| Meadow marsh           | 0              | 2         | 0          | 0           | 0        | <b>3</b>     | 0          | 1          | 1             | 0            | 0          | 7     |
| Open water             | 0              | 0         | 0          | 0           | 0        | 0            | <b>44</b>  | 0          | 10            | 0            | 0          | 54    |
| <i>Phragmites</i>      | 0              | 1         | 6          | 0           | 0        | 19           | 0          | <b>41</b>  | 3             | 8            | 0          | 78    |
| Shallow marsh          | 1              | 0         | 7          | 0           | 4        | 7            | 0          | 0          | <b>13</b>     | 1            | 0          | 33    |
| Trees/shrubs           | 4              | 0         | 0          | 0           | 1        | 0            | 0          | 6          | 0             | <b>9</b>     | 0          | 20    |
| Total                  | 74             | 24        | 121        | 28          | 16       | 31           | 48         | 50         | 27            | 18           | <b>437</b> |       |

Number of correctly classified pixels for each land cover class are given in bold text

**Table 6** Error Matrix for Landsat 8 (2015 July 21) for the Big Creek (number of pixels)

| Classification results | Reference data |           |            |             |           |              |            |                   |               |              |            | Total |
|------------------------|----------------|-----------|------------|-------------|-----------|--------------|------------|-------------------|---------------|--------------|------------|-------|
|                        | Agriculture    | Beach     | Cattail    | Constructed | Floating  | Meadow marsh | Open water | <i>Phragmites</i> | Shallow marsh | Trees/shrubs | Total      |       |
| Agriculture            | <b>70</b>      | 0         | 0          | 0           | 0         | 0            | 0          | 0                 | 0             | 0            | 0          | 70    |
| Beach                  | 0              | <b>19</b> | 1          | 1           | 0         | 0            | 0          | 0                 | 0             | 0            | 0          | 21    |
| Cattail                | 0              | 0         | <b>120</b> | 0           | 0         | 8            | 1          | 2                 | 0             | 0            | 0          | 131   |
| Constructed            | 0              | 1         | 0          | <b>27</b>   | 0         | 0            | 0          | 0                 | 0             | 0            | 0          | 28    |
| Floating               | 0              | 0         | 0          | 0           | <b>10</b> | 0            | 0          | 0                 | 0             | 0            | 0          | 10    |
| Meadow marsh           | 0              | 2         | 0          | 0           | 0         | <b>13</b>    | 0          | 0                 | 0             | 0            | 0          | 15    |
| Open water             | 0              | 0         | 0          | 0           | 2         | 0            | <b>43</b>  | 0                 | 4             | 0            | 0          | 49    |
| <i>Phragmites</i>      | 0              | 2         | 0          | 0           | 0         | 2            | 2          | <b>48</b>         | 0             | 0            | 0          | 54    |
| Shallow marsh          | 0              | 0         | 0          | 0           | 4         | 4            | 2          | 0                 | <b>19</b>     | 0            | 0          | 29    |
| Trees/shrubs           | 4              | 0         | 0          | 0           | 0         | 4            | 0          | 0                 | 4             | <b>18</b>    | 0          | 30    |
| Total                  | 74             | 24        | 121        | 28          | 16        | 31           | 48         | 50                | 27            | 18           | <b>437</b> |       |

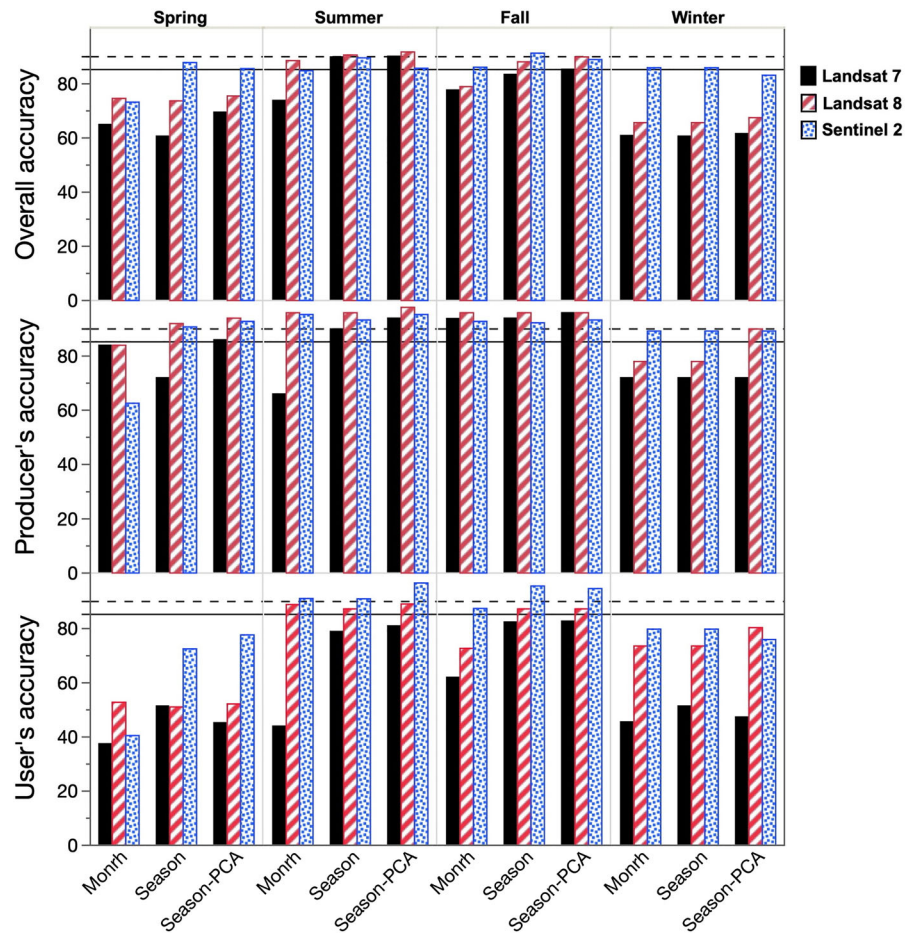
Number of correctly classified pixels for each land cover class are given in bold text

**Table 7** Error Matrix for Sentinel 2 (2016 July 26) for the Big Creek (number of pixels)

| Class             | Reference data |           |            |             |           |              |            |                   |               |              |             | Total |
|-------------------|----------------|-----------|------------|-------------|-----------|--------------|------------|-------------------|---------------|--------------|-------------|-------|
|                   | Agriculture    | Beach     | Cattail    | Constructed | Floating  | Meadow marsh | Open water | <i>Phragmites</i> | Shallow marsh | Trees/shrubs | Total       |       |
| Agriculture       | <b>167</b>     | 0         | 0          | 0           | 0         | 1            | 0          | 0                 | 0             | 0            | 0           | 168   |
| Beach             | 0              | <b>78</b> | 0          | 8           | 0         | 0            | 0          | 0                 | 0             | 0            | 0           | 86    |
| Cattail           | 0              | 0         | <b>347</b> | 0           | 0         | 15           | 0          | 12                | 8             | 0            | 0           | 382   |
| Constructed       | 0              | 5         | 0          | <b>112</b>  | 0         | 0            | 0          | 0                 | 0             | 0            | 0           | 117   |
| Floating          | 0              | 0         | 1          | 0           | <b>28</b> | 0            | 0          | 0                 | 0             | 0            | 0           | 29    |
| Meadow marsh      | 0              | 0         | 71         | 0           | 0         | <b>97</b>    | 0          | 0                 | 0             | 0            | 0           | 168   |
| Open water        | 4              | 0         | 0          | 1           | 0         | 0            | <b>197</b> | 0                 | 37            | 0            | 0           | 239   |
| <i>Phragmites</i> | 0              | 0         | 16         | 0           | 0         | 4            | 0          | <b>246</b>        | 1             | 3            | 0           | 270   |
| Shallow marsh     | 0              | 0         | 1          | 0           | 12        | 2            | 16         | 0                 | <b>48</b>     | 8            | 0           | 87    |
| Trees/shrubs      | 13             | 0         | 0          | 0           | 0         | 1            | 0          | 0                 | 0             | <b>19</b>    | 0           | 33    |
| Total             | 184            | 83        | 436        | 121         | 40        | 120          | 213        | 258               | 94            | 30           | <b>1579</b> |       |

Number of correctly classified pixels for each land cover class are given in bold text

**Fig. 5** Comparison of Overall, Producer's and User's accuracies for automated classifications of three different satellite images of Big Creek Wetland. Accuracies are sorted by three different methods. Month refers to a single month for a season. Solid line indicates 85% accuracy whereas the dotted line refers to 90% accuracy



imagery by identifying the best phenological period during which the plants produced their most distinguishable signature compared to background land-cover classes (especially cattails and meadow marsh). Variation in surface reflectance of marsh vegetation associated with phenological changes over the year were captured in remotely sensed imagery (Zhang et al. 2003; Tuanmu et al. 2010). We were able to monitor these phenological changes in our wetlands using satellite data with moderate spatial resolution that included Landsat 7, 8 and Sentinel 2. Classified images of all three satellite platforms resulted in maps of *Phragmites* of acceptable accuracy (> 80% average accuracy of overall and *Phragmites* user's and producer's accuracy) when classifications were performed on images acquired in late summer or fall. Of all three satellites, the accuracy of classified Landsat 7 images was lowest, in part because of data gaps; Landsat 8 provided the highest overall accuracy while

Sentinel 2 provided highest *Phragmites* user's and producer's accuracy.

The data source, classification algorithm, and use of timely ground reference data can all affect the accuracy of image classification, especially for fine-scale species mapping. Ensuring that ground reference collection and image acquisition are completed in the same year is probably most important, especially when complex vegetation features such as wetlands are considered. We obtained lower classification accuracy overall for RBM than for BCNWA using either Landsat 8 or Sentinel 2, partly because of mismatched timing between field surveys (all collected in 2011) and image acquisition (2014 for Landsat 8 and 2016 for Sentinel 2 images, respectively). Landsat 7 images, on the other hand, provided higher classification accuracy because the satellite images had been acquired in 2009, 2010 and 2011, closer to the time of field surveys. Another reason for the poorer

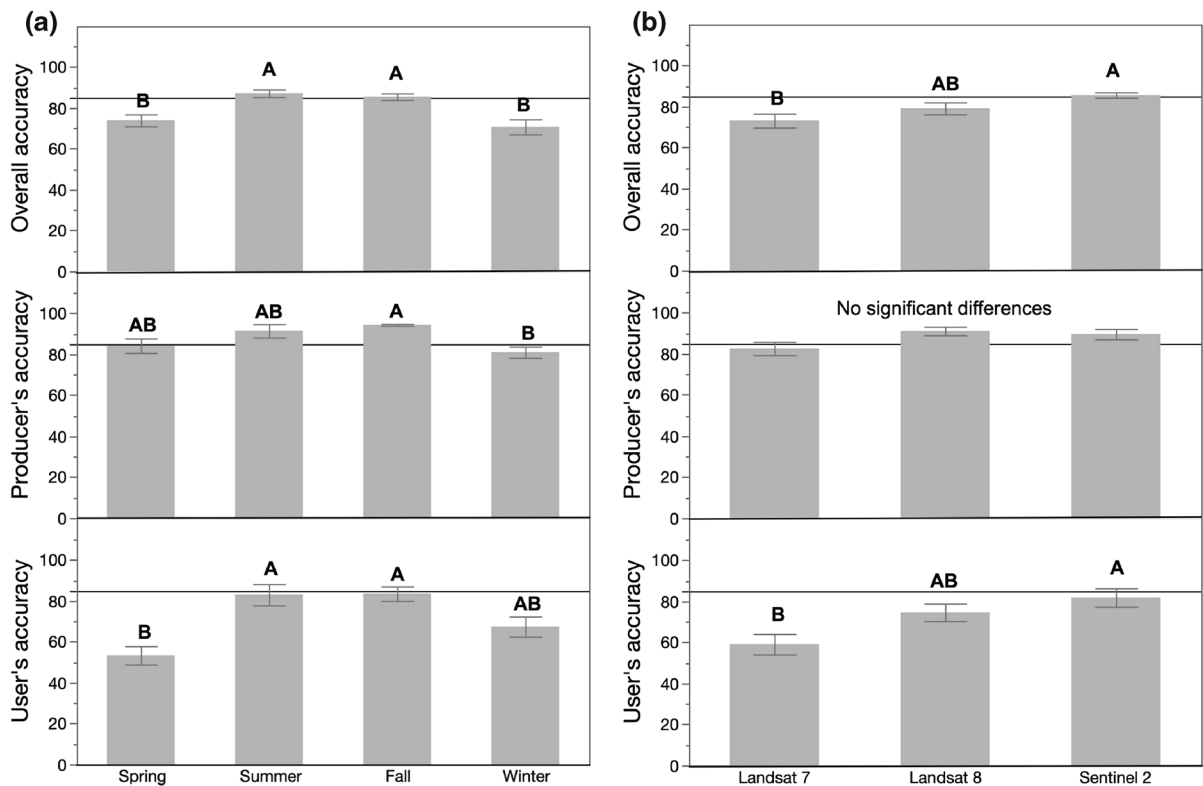


**Fig. 6** Results of ANOVA comparing *Phragmites* user's, producer's and overall accuracies across **a** four seasons and **b** satellite sensors. Similar letters join statistically homogeneous means in each panel as indicated by a Tukey's comparison of multiple means

accuracies for Landsat 8 and Sentinel 2 was because a control program had been implemented in the fall of 2011, and many of the *Phragmites* stands that were present in the 2011 field surveys had been eradicated and were no longer present in the 2014 and 2016 images. We tried to improve accuracy in two ways, first by manually delineating *Phragmites* stands in a 2015 SWOOP image to provide more appropriate ground reference data for the 2014 and 2016 satellite images and secondly, by accounting for treatment locations. Due to the inconsistency of image and field reference data collection time, however, we can only use the RBM site to apply methodology developed for the BCNWA site, and we believe that the mismatch of field reference and image dates for RBM did not materially affect conclusions drawn from the BCNWA data.

Marcaccio and Chow-Fraser (2016) found various degrees of accuracies when they compared four mapping options and data sources for mapping BCNWA. In the first option, Ontario Ministry of Natural Resources and Forestry (OMNRF) classified

Landsat data using an NDVI-based hierarchical image object-based decision tree (Young et al. 2011). The data sources were Landsat 5 and 7 images acquired in summer 1993, 1999, and 2010; Marcaccio and Chow-Fraser obtained an overall accuracy of 57%, with associated *Phragmites* producer's and user's accuracy of 56% and 77% respectively for this option. This is lower than our results where the overall accuracy was 75 and 86% for Landsat 7, 71% and 88% for Landsat 8, and > 80% *Phragmites* accuracy for most of the cases with the SVM classification. This is likely because the OMNRF study did not include any ground reference in their classification whereas here we used a number of ground reference points for both classification and accuracy assessment.

The second option in Marcaccio and Chow-Fraser's study involved use of PALSAR (Phased Array type L-band Synthetic Aperture Radar; Bourgeau-Chavez et al. 2015). In this approach, all landcover within a 10 km buffer of the Great Lakes shoreline was mapped, including several classes of emergent vegetation, particularly *Phragmites*. Landsat 7 data

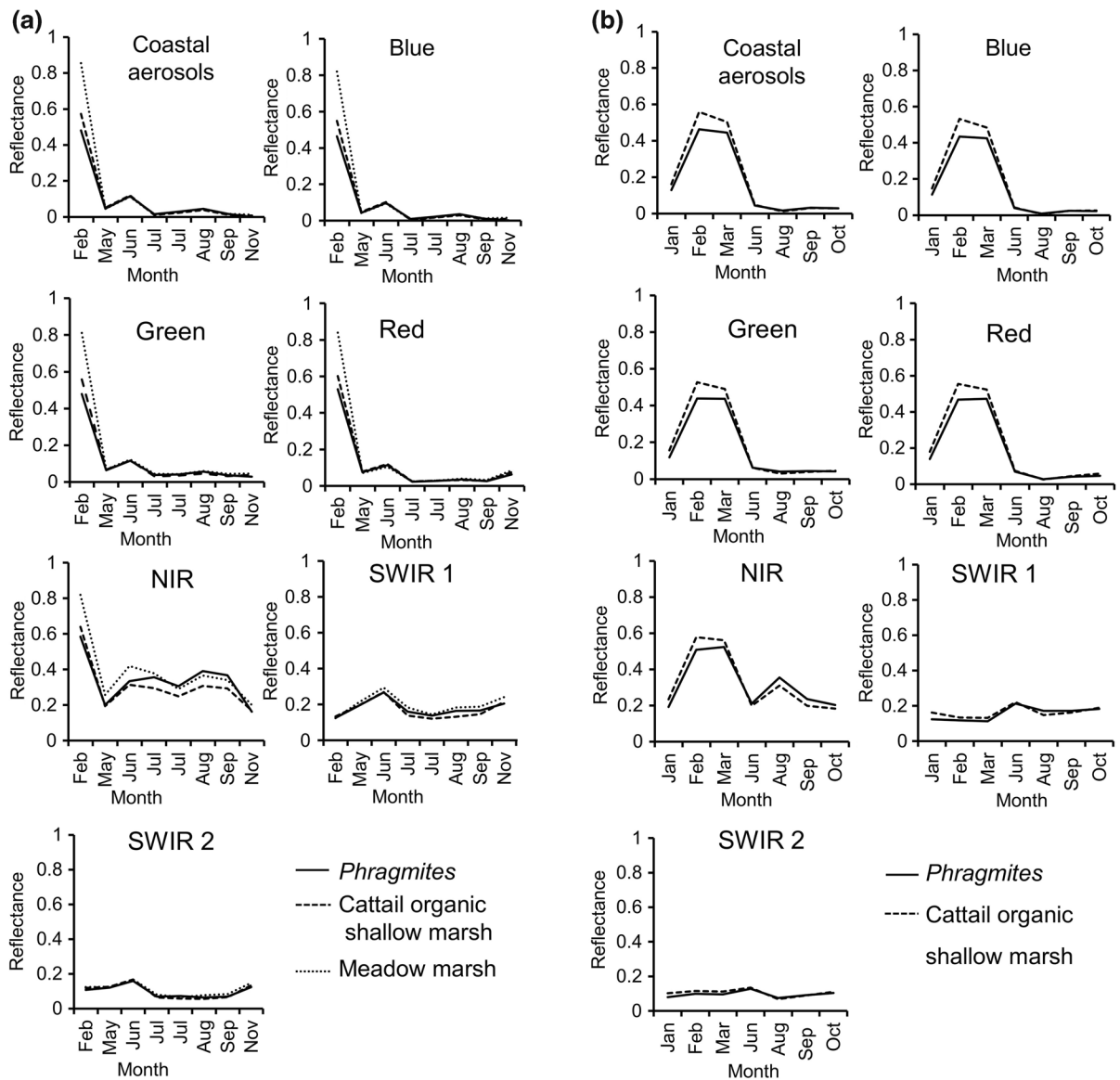


**Fig. 7** Monthly changes in reflectance of **a** *Phragmites*, cattail organic shallow marsh and meadow marsh for BCNWA site and **b** *Phragmites* and cattail for RBM site for the 7 bands of Landsat 8

collected in spring, summer and fall from 2008 to 2011 had been used to delineate landscape features; the authors used random forests isodata and the maximum likelihood classification methods, as well as field reference data for both classification and accuracy assessment. When this approach was applied to BCNWA, Marcaccio and Chow-Fraser (2016) obtained 77% overall accuracy, and *Phragmites* producer's and user's accuracies of 86% and 77%, respectively. This compares favorably with the 77%

that we obtained for producer's and user's accuracy in this study. Although radar data appear to be advantageous for mapping *Phragmites* and the PALSAR data are now freely available, we will not be able to use these image data for mapping updates because the mission ended in 2011.

Marcaccio and Chow-Fraser (2018) have used the image object-oriented classification method for SWOOP images collected in spring 2006, 2010, and 2015 to map *Phragmites* along major highways of

**Table 8** P-Values for selection of most contributing bands for the *Phragmites* signature using one-way ANOVA and Tukey's test

| BCNWA                          |         | Number of significant p-values |              |              |              |              |              |              |   |
|--------------------------------|---------|--------------------------------|--------------|--------------|--------------|--------------|--------------|--------------|---|
| Band                           | Classes | Feb                            | May          | Jun          | Jul          | Aug          | Sep          | Nov          |   |
| Coastal aerosols               | P–C     | 0.076                          | <b>0.021</b> | 0.579        | 0.100        | 0.060        | 0.051        | 0.189        | 1 |
|                                | P–M     | <b>0.000</b>                   | 0.821        | 0.200        | 0.120        | 0.240        | 0.089        | <b>0.010</b> | 2 |
| Blue                           | P–C     | 0.067                          | 0.240        | 0.984        | 0.200        | 0.074        | <b>0.001</b> | 0.052        | 1 |
|                                | P–M     | <b>0.000</b>                   | 0.996        | 0.882        | 1.000        | 0.989        | <b>0.004</b> | 0.056        | 2 |
| Green                          | P–C     | 0.073                          | <b>0.040</b> | 0.631        | <b>0.002</b> | <b>0.041</b> | <b>0.000</b> | 0.082        | 4 |
|                                | P–M     | <b>0.000</b>                   | 0.634        | 0.114        | 0.102        | 0.142        | 0.377        | <b>0.003</b> | 2 |
| Red                            | P–C     | 0.053                          | 0.127        | 0.815        | <b>0.004</b> | <b>0.009</b> | 0.098        | 0.074        | 2 |
|                                | P–M     | <b>0.000</b>                   | 0.445        | <b>0.044</b> | 0.994        | 0.113        | 0.012        | 0.057        | 2 |
| NIR                            | P–C     | <b>0.006</b>                   | 0.963        | 0.621        | <b>0.000</b> | <b>0.000</b> | <b>0.000</b> | 0.500        | 4 |
|                                | P–M     | <b>0.000</b>                   | 0.239        | 0.191        | <b>0.022</b> | <b>0.022</b> | 0.248        | 0.138        | 3 |
| SWIR 1                         | P–C     | 0.081                          | 0.378        | 0.97         | <b>0.000</b> | <b>0.000</b> | <b>0.003</b> | 0.47         | 3 |
|                                | P–M     | <b>0.048</b>                   | 0.831        | 0.915        | 0.788        | 0.994        | 0.134        | 0.398        | 1 |
| SWIR 2                         | P–C     | <b>0.000</b>                   | 0.214        | 0.638        | <b>0.000</b> | <b>0.000</b> | <b>0.003</b> | 0.219        | 4 |
|                                | P–M     | <b>0.000</b>                   | 0.985        | 0.998        | <b>0.000</b> | 0.239        | 0.134        | 0.166        | 2 |
| Number of significant p-values | P–C     | 2                              | 2            | 0            | 5            | 5            | 5            | 0            |   |
|                                | P–M     | 7                              | 0            | 1            | 2            | 1            | 1            | 2            |   |
| RBM                            |         |                                |              |              |              |              |              |              |   |
|                                | Classes | Jan                            | Feb          | Mar          | Jun          | Aug          | Sep          | Oct          |   |
| Coastal aerosols               | P–C     | 0.124                          | 0.172        | 0.398        | 0.331        | 0.109        | 0.435        | 0.655        | 0 |
| Blue                           | P–C     | 0.384                          | 0.154        | 0.383        | 0.377        | 0.377        | 0.748        | 0.225        | 0 |
| Green                          | P–C     | 0.325                          | 0.174        | 0.406        | 0.850        | <b>0.007</b> | 0.137        | 0.582        | 1 |
| Red                            | P–C     | 0.290                          | 0.173        | 0.413        | 0.653        | 0.687        | 0.236        | <b>0.013</b> | 1 |
| NIR                            | P–C     | 0.159                          | 0.167        | 0.462        | 0.447        | <b>0.021</b> | <b>0.003</b> | <b>0.045</b> | 3 |
| SWIR 1                         | P–C     | 0.058                          | 0.077        | 0.056        | 0.630        | <b>0.001</b> | 0.128        | 0.476        | 1 |
| SWIR 2                         | P–C     | 0.061                          | 0.120        | 0.100        | 0.560        | 0.103        | 0.698        | 0.287        | 0 |
| Number of significant p-values | P–C     | 0                              | 0            | 0            | 0            | 3            | 1            | 2            |   |

Statistically significant values are given in bold text

P–C *Phragmites* and Cattail organic shallow marsh comparison and P–M *Phragmites* and meadow marsh comparison

southern and central Ontario. When this approach was applied to mapping BCNWA, the overall classification accuracy was 62%, while the producer's accuracy was 90% and the user's accuracy was 58%. Although the 20 cm spatial resolution has obvious advantages, the SWOOP images are only available every 5 years. Marcaccio et al. (2016) also used UAV data (spatial resolution of 8 cm) to manually delineate land cover types based on extensive field surveys of the BCNWA. This method provided the highest user's and producer's accuracy of 100% while the overall accuracy

was 87%. The method was highly accurate but also the most labor intensive.

Stratoulis et al. (2015) developed a simulation of the bands of Sentinel 2 based on the satellite's response function and airborne hyperspectral data collected from the sensor AISA for lakeshore mapping at Lake Balaton, Hungary. They also used the SVM classification and have reported that Sentinel 2 can perform satisfactorily in classifying wetland ecosystems, including *Phragmites*. They suggested, however, that the *Phragmites* mapping accuracy could be reduced if higher inter-class spectral variability were

**Table 9** Accuracy (%) values for Landsat 8 July images when one band is excluded at a time

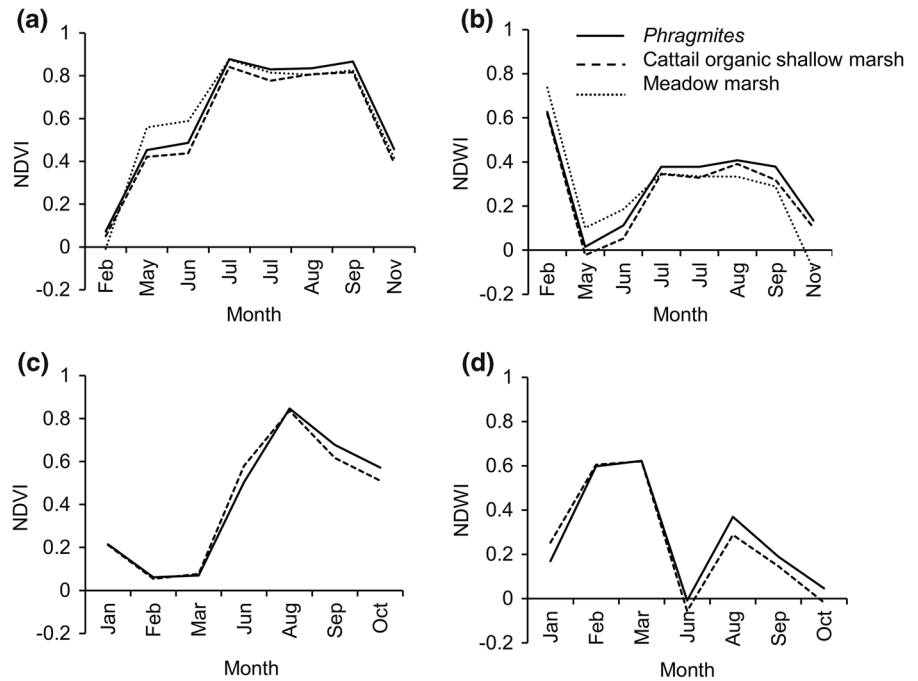
| Image          | BCNWA        |            |              | Average      | RBM          |              |              | Average      |
|----------------|--------------|------------|--------------|--------------|--------------|--------------|--------------|--------------|
|                | Overall      | Producer's | User's       |              | Overall      | Producer's   | User's       |              |
| With 7 bands   | 88.56        | 96.00      | 92.31        | 92.29        | 75.00        | 79.59        | 73.58        | 76.06        |
| Without band 1 | 87.64        | 96.00      | 90.56        | 91.40        | 74.58        | 79.51        | 72.55        | 75.55        |
| Without band 2 | 88.10        | 96.00      | 90.57        | 91.56        | 75.00        | <b>77.55</b> | 72.70        | 75.08        |
| Without band 3 | <b>86.27</b> | 96.00      | <b>88.71</b> | <b>90.33</b> | <b>72.46</b> | <b>73.47</b> | <b>71.26</b> | <b>72.40</b> |
| Without band 4 | 88.10        | 96.00      | 90.57        | 91.56        | 74.15        | 79.59        | 73.58        | 75.78        |
| Without band 5 | <b>85.58</b> | 96.00      | <b>85.71</b> | <b>89.10</b> | 74.15        | 77.55        | 71.70        | 74.47        |
| Without band 6 | <b>86.19</b> | 96.00      | <b>85.12</b> | <b>89.10</b> | 73.30        | <b>71.43</b> | <b>70.00</b> | <b>71.58</b> |
| Without band 7 | 88.10        | 96.00      | 90.57        | 91.56        | 75.00        | 79.51        | 72.41        | 75.85        |

| Difference of accuracy from classification accuracy of all seven bands |             |      |             |             |             |             |             |             |
|--|-------------|------|-------------|-------------|-------------|-------------|-------------|-------------|
| Without band 1   | 0.92        | 0.00 | 1.75        | 0.89        | 0.42        | 0.08        | 1.03        | 0.51        |
| Without band 2   | 0.46        | 0.00 | 1.74        | 0.73        | 0.00        | <b>2.04</b> | 0.88        | 0.98        |
| Without band 3   | <b>2.29</b> | 0.00 | <b>3.60</b> | 1.96        | <b>2.54</b> | <b>6.12</b> | <b>2.32</b> | <b>3.66</b> |
| Without band 4   | 0.46        | 0.00 | 1.74        | 0.73        | 0.85        | 0.00        | 0.00        | 0.28        |
| Without band 5   | <b>2.98</b> | 0.00 | <b>6.6</b>  | <b>3.19</b> | 0.85        | <b>2.04</b> | 1.88        | 1.59        |
| Without band 6   | <b>2.37</b> | 0.00 | <b>7.19</b> | <b>3.19</b> | 1.70        | <b>8.16</b> | <b>3.58</b> | <b>4.48</b> |
| Without band 7   | 0.46        | 0.00 | 1.74        | 0.73        | 0.00        | 0.08        | 1.17        | 0.21        |

Producer's and User's accuracy pertain to invasive *Phragmites*. Overall accuracy pertains to all classified classes  
 Bands that reduce the accuracy more than 2% when excluded is bolded

**Fig. 8** Monthly changes in **a** NDVI and **b** NDWI for BCNWA and **c** NDVI and **d** NDWI for RBM for *Phragmites*, cattail organic shallow marsh and meadow marsh



**Table 10** P-Values for monthly changes of NDVI and NDWI of *Phragmites*, cattail organic shallow marsh, and meadow marsh using one-way ANOVA and Tukey's test

| Band                           | BCNWA   |              |              |              |              |              |              |              | Number of significant p-values |
|--------------------------------|---------|--------------|--------------|--------------|--------------|--------------|--------------|--------------|--------------------------------|
|                                | Classes | Feb          | May          | Jun          | Jul          | Aug          | Sep          | Nov          |                                |
| NDVI                           | P–C     | 0.060        | 0.550        | 0.304        | 0.140        | <b>0.003</b> | <b>0.002</b> | <b>0.003</b> | 3                              |
|                                | P–M     | <b>0.000</b> | <b>0.000</b> | <b>0.000</b> | 0.992        | 0.079        | <b>0.048</b> | 0.306        | 4                              |
| NDWI                           | P–C     | 0.078        | 0.254        | <b>0.010</b> | <b>0.000</b> | <b>0.017</b> | <b>0.000</b> | 0.181        | 4                              |
|                                | P–M     | <b>0.000</b> | 0.087        | 0.422        | <b>0.000</b> | <b>0.000</b> | <b>0.000</b> | 0.730        | 4                              |
| Number of significant p-values | P–C     | 0            | 0            | 1            | 1            | 2            | 2            | 1            |                                |
|                                | P–M     | 2            | 1            | 1            | 1            | 1            | 2            | 0            |                                |
| RBM                            |         |              |              |              |              |              |              |              | Number of significant p-values |
|                                | Classes | Jan          | Feb          | Mar          | Jun          | Aug          | Sep          | Oct          |                                |
| NDVI                           | P–C     | 0.914        | 0.706        | 0.727        | <b>0.045</b> | 0.720        | <b>0.029</b> | <b>0.030</b> | <b>3</b>                       |
| NDWI                           | P–C     | 0.169        | 0.862        | 0.959        | 0.136        | <b>0.000</b> | 0.058        | 0.053        | 1                              |
| Number of significant p-values | P–C     | 0            | 0            | 0            | 1            | 1            | 1            | 1            |                                |

statistically significant values are given in bold text

P–C *Phragmites* and Cattail organic shallow marsh comparison and P–M *Phragmites* and meadow marsh comparison

present. They first predicted the strong capability of Sentinel 2 imagery for fine-habitat monitoring for species such as *Phragmites*. Our study has confirmed this prediction and showed that Sentinel 2 imagery can be used to map wetlands with relatively high accuracies for both *Phragmites* and other land classes.

All previous *Phragmites* mapping techniques have demonstrated various pros and cons in terms of data sources and availability, mapping technique, and accuracy. Our method is advantageous over these published mapping options because we use freely available data within relatively short time intervals, with sensors that are still available (and will be for the foreseeable future). Moreover, mapping accuracy has been high, both with respect to overall accuracy as well as for *Phragmites* alone. The one limitation of this approach is the low spatial resolution, which limits the accuracy of mapping small stands of *Phragmites* or mixed assemblages of *Phragmites* with other emergent or meadow taxa. Our method also requires a large number of ground reference locations, collected in the same year when the image is acquired. This approach relies on availability of cloud-free images and can be an insurmountable problem as we discovered for RBM, when we could not find any cloud-free images in 2011. Nevertheless, the relatively high accuracy, zero cost of data acquisition and

continuous availability of images, we believe our novel approach is best suited to tracking changes in distribution of *Phragmites* when monitoring for effectiveness of treatment programs.

The reflectance signature of a plant depends on many factors (Knipling 1970.) Reflectance in the visible region is mainly affected by the types of plant pigments (primarily chlorophyll) and their concentration, and some effect by carotenoids, xanthophylls, and anthocyanin. Leaf internal structure, specifically the cellular arrangement and layers, cell wall cellulose structures, and air cavities can affect the reflectance in the NIR region (Wilstetter and Stoll 1918; Mestre 1935; Sinclair et al. 1968). Reflectance in the SWIR region is strongly influenced by the water content in plant tissues, especially in wavelengths 1.45  $\mu\text{m}$  and 1.94  $\mu\text{m}$  (Fabre et al. 2011). Besides properties of a single leaf, other factors that can affect the plant's reflectance signature includes features such as leaf orientation, shadows, illumination angle, leaf density, and the size of leaves and the non-foliage background features such as soil (for the terrestrial species) or water (for the wetland species) (Knipling 1970). Hence, species with similar morphology and anatomy may share various degrees of similarity in reflectance signatures.

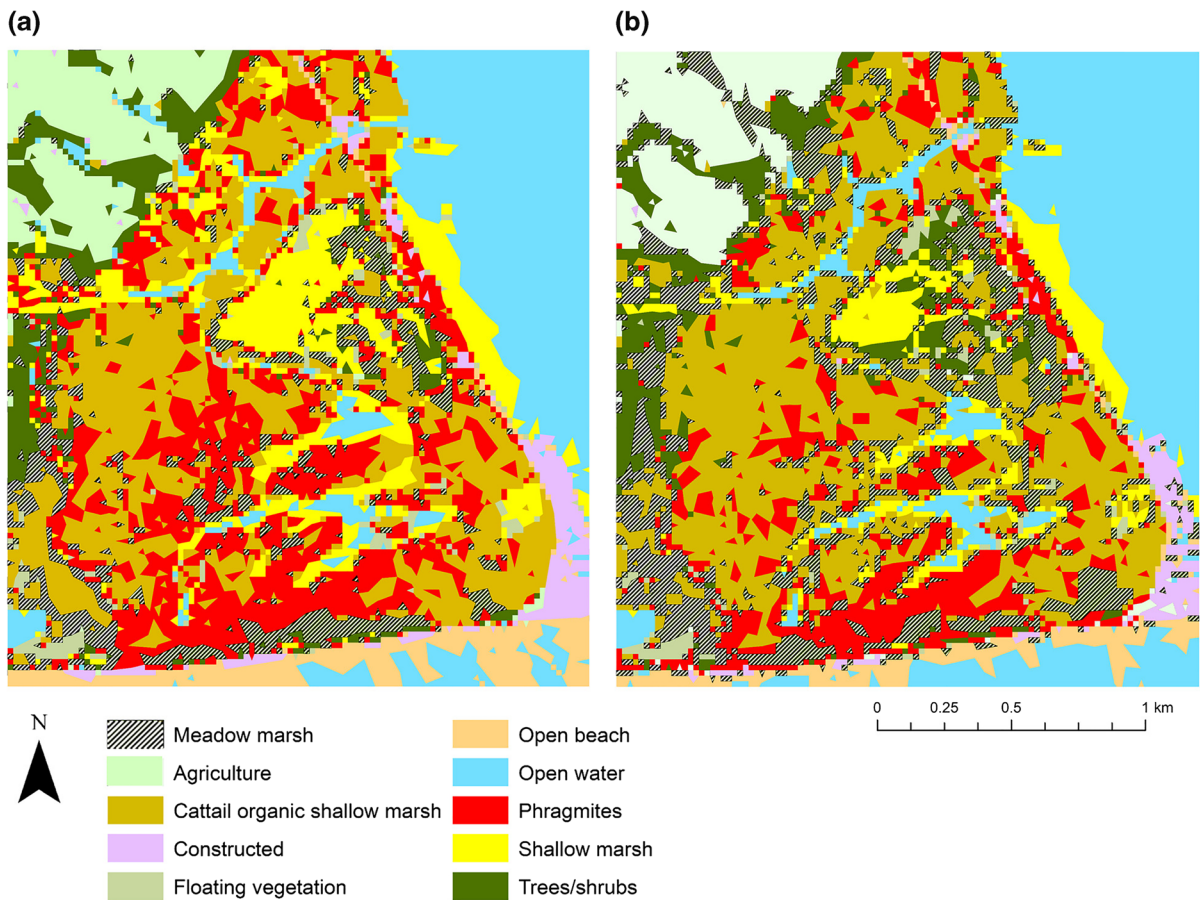


**Fig. 9** Landsat 8 images for mapping meadow marsh **a** using only July image and **b** using July image after masking meadow marsh with February image

Both cattail and meadow marsh are highly confused with *Phragmites* in our classification approach. All three classes occupy similar habitats where the plants are partially submerged. Hence the background reflectance has the same effect on them and result in somewhat similar signals. For example, cattail and *Phragmites* both share similar morphological traits, being tall, unbranched shoots that form dense monospecific stands and have approximately similar leaf arrangement (Bellavance and Brisson 2010). Hence both species produced very similar reflectance signatures that caused confusion in image classification. There were differences, however, in how the two species senesced; cattail started yellowing by the end of July while *Phragmites* remained green until early September. Moreover, *Phragmites* produced its unique, and large inflorescence by the end of summer and throughout the fall. Hence *Phragmites* and cattail

exhibited highest separability during late summer to fall, and this led to increased mapping accuracy. The NDVI time-series analysis mirrored this since both classes had a similar pattern throughout the year except in July to September, when they had highest divergence. We obtained significant separation between cattail and *Phragmites* in June to September using NDWI values and this indicates that plant-water features may also play a role in discriminating between these two classes.

The meadow marsh produced a relatively complicated signature, that reflected the assemblage of different plant species, including various grasses, sedges, emergent shrubs, and upland plant species (Wilcox n.d.). Furthermore, the meadow marsh community undergoes occasional flooding, and this leads to even more variability in their reflectance signals throughout the year. Therefore, the meadow marsh

signal is confused not only with *Phragmites*, but also with other wetland landcover classes such as cattail and shallow marsh. In February, however, the meadow marsh tends to be completely covered by snow while the taller *Phragmites* and cattail stalks are only partially covered in snow. This difference in February can be used to increase the separability among these three classes. Although separability between *Phragmites* and meadow marsh was higher during the winter, the reflectance signal of meadow marsh still overlapped with that of other snow-cover features such as shallow marsh, beach, and frozen shallow water. Hence the overall accuracy was low. Additionally, the degree of separability between *Phragmites* and meadow marsh during the winter may depend on the amount of snow accumulation. There was a significant difference in NDVI between *Phragmites* and meadow marsh from February to July and significant NDWI difference from July to September. With respect to invasive *Phragmites* and meadow marsh, however, there was no clear pattern in NDVI and NDWI, and hence these may not help to separate these classes to improve mapping accuracy.

Many studies have explored the use of combined images collected in different seasons and have reported improved classification accuracy (Oetter et al. 2001; Guerschman et al. 2003; Tottrup 2004; Lu and Weng 2007). Use of multi-temporal images in classification not only incorporates fine phenological changes in the spectral data, but also helps to exclude the effect of the sun's angle and to provide a unique spectral response pattern (Tottrup 2004). We expected that use of multitemporal images for wetland classification may be useful in overcoming the effect of varying water levels within each season; however, we did not observe any evidence that overall classification accuracy would increase significantly by combining multiple images. According to Tottrup (2004) the acquisitions should not be too close in time as there are no clear changes in phenology and the sun's angle within a single season. Our results may have been different if we had combined multiple images for the same seasons; however, we did not explore this as our main objective was to determine the phenological states of *Phragmites* that produced the most unique reflectance signature for mapping. Finally, we should point out that use of a PCA to reduce the effect of redundant data did not yield a significant increase in accuracy as expected.

## Conclusions

We accurately mapped large *Phragmites* patches in wetlands using Landsat and Sentinel 2 images acquired in late summer through fall, in combination with the SVM classification method. To achieve high classification accuracy, our protocol requires a large number of ground reference locations to be established. Our results indicate that the green, NIR, and SWIR bands are most useful in development of the unique *Phragmites* reflectance signal during this period. We believe that the prolonged greenness of *Phragmites* when compared to other wetland vegetation, large, distinct inflorescence, and the water content of *Phragmites* during this period helps to produce the unique reflectance signature. Also, the prolonged greenness of *Phragmites* when compared to other classes help in the mapping process. Cattail and meadow marsh were the most confused classes with *Phragmites*, likely because all three landcover classes occupy similar habitats and have similar morphological features.

Although *Phragmites* best separated out from cattails and other classes in July to September, meadow marsh separated out best in February. Therefore, we recommend the use of February (snow covered) images in combination with summer time images to reduce the confusion among these three classes. This may be more useful when maps are produced for management purposes when the primary goal is to accurately map invaded areas. Use of multitemporal images for each season did not increase classification accuracy.

Overall, our study explored the use of freely available satellite data for mapping invasive *Phragmites*, which has become a serious management issue. Despite the moderate spatial resolution, images acquired in the correct phenological state can increase classification accuracy. Our novel approach provides a cost-effective and accurate *Phragmites* mapping method for different types of wetland ecosystems, when *Phragmites* needs to be frequently monitored and managed across large spatial extents.

**Acknowledgements** Partial funding for this study came from a grant to PC-F from the Highway Infrastructure Innovation Funding Program from the Ministry of Transportation of Ontario. We thank C. Markle and J. Marcaccio for their assistance in assembling relevant data for this study. We are

grateful to the helpful comments provided by anonymous reviewers on an earlier draft of this manuscript.

## References

- Adam E, Mutanga O, Rugege D (2010) Multispectral and hyperspectral remote sensing for identification and mapping of wetland vegetation: a review. *Wetl Ecol Manag* 18:281–296
- Ashley EP, Robinson JT (1996) Road mortality of amphibians, reptiles and other wildlife on the Long Point Causeway, Lake Erie, Ontario. *Can Field Nat* 110:403–412
- Bellavance M-E, Brisson J (2010) Spatial dynamics and morphological plasticity of common reed (*Phragmites australis*) and cattails (*Typha* sp.) in freshwater marshes and roadside ditches. *Aquat Bot* 93:129–134
- Bostater CR, Ghir T, Bassetti L, Hall C, Reyeier E, Lowers R, Holloway-Adkins K, Virmstein R (2004) Hyperspectral remote sensing protocol development for submerged aquatic vegetation in shallow waters. Proceedings of SPIE 5233, Remote Sensing of the Ocean and Sea Ice 2003; Event: Remote Sensing, 2003, Barcelona, Spain 5233:199–215. <https://doi.org/10.1117/12.541191>
- Bourgeau-Chavez L, Endres S, Battaglia M et al (2015) Development of a bi-national Great Lakes coastal wetland and land use map using three-season PALSAR and Landsat imagery. *Remote Sens* 7:8655–8682
- Chambers RM, Meyerson LA, Saltonstall K (1999) Expansion of *Phragmites australis* into tidal wetlands of North America. *Aquat Bot* 64:261–273
- Dalponete M, Bruzzone L, Gianelle D (2008) Fusion of hyperspectral and LIDAR remote sensing data for classification of complex forest areas. *IEEE Trans Geosci Remote Sens* 46:1416–1427
- Delegido J, Verrelst J, Alonso L, Moreno J (2011) Evaluation of sentinel-2 red-edge bands for empirical estimation of green LAI and chlorophyll content. *Sensors* 11:7063–7081
- Dewey SA, Price KP, Ramsey D (1991) Satellite remote sensing to predict potential distribution of dyers woad (*Isatis tinctoria*). *Weed Technol* 5:479–484
- Environment and Climate Change Canada (2011) Big Creek National Wildlife Area. In: aem. <https://www.canada.ca/en/environment-climate-change/services/national-wildlife-areas/locations/big-creek.html>. Accessed 26 Mar 2018
- Everitt JH, Anderson GL, Escobar DE et al (1995) Use of remote sensing for detecting and mapping leafy spurge (*Euphorbia esula*). *Weed Technol* 9:599–609
- Everitt JH, Escobar DE, Alaniz MA et al (1996) Using spatial information technologies to map Chinese tamarisk (*Tamarix chinensis*) infestations. *Weed Sci* 44:194–201
- Everitt JH, Escobar DE, Davis MR (2001) Reflectance and image characteristics of selected noxious rangeland species. *J Range Manag* 54:208–208
- Fabre S, Lesaignoux A, Olioso A, Briottet X (2011) Influence of water content on spectral reflectance of leaves in the 3–15  $\mu\text{m}$  domain. *IEEE Geosci Remote Sens Lett* 8:143–147
- Sanchez-Flores E, Rodriguez-Gallegos H, Yool SR (2008) Plant invasions in dynamic desert landscapes. A field and remote sensing assessment of predictive and change modeling. *J Arid Environ* 72(3):189–206
- Frampton WJ, Dash J, Watmough G, Milton EJ (2013) Evaluating the capabilities of Sentinel-2 for quantitative estimation of biophysical variables in vegetation. *ISPRS J Photogramm Remote Sens* 82:83–92
- Fuller DO (2005) Remote detection of invasive *Melaleuca* trees (*Melaleuca quinquenervia*) in South Florida with multi-spectral IKONOS imagery. *Int J Remote Sens* 26:1057–1063
- Gao J, Liu Y (2008) Mapping of land degradation from space: a comparative study of Landsat ETM+ and ASTER data. *Int J Remote Sens* 29(14):4029–4043
- Gibert JM (2015) Rondeau Provincial Park Invasive *Phragmites* Management Program 2008–2014 Summary Report and Recommended Next Steps (Unpublished manuscript)
- Glass WR, Corkum LD, Mandrak NE (2012) Spring and summer distribution and habitat use by adult threatened spotted gar in Rondeau Bay, Ontario, using radiotelemetry. *Trans Am Fish Soc* 141:1026–1035
- Gualtieri JA, Crompton RF (1999) Support vector machines for hyperspectral remote sensing classification. In: 27th AIPR Workshop: Advances in Computer-Assisted Recognition. International Society for Optics and Photonics, pp 221–233
- Guerschman JP, Paruelo JM, Bella CD et al (2003) Land cover classification in the Argentine Pampas using multi-temporal Landsat TM data. *Int J Remote Sens* 24:3381–3402
- Harris Geospatial (2018) Fast Line-of-sight Atmospheric Analysis of Hypercubes (FLAASH) <https://www.harrisgeospatial.com/docs/FLAASH.html> Accessed 20 June 2018
- Hestir EL, Khanna S, Andrew ME et al (2008) Identification of invasive vegetation using hyperspectral remote sensing in the California Delta ecosystem. *Remote Sens Environ* 112:4034–4047. <https://doi.org/10.1016/j.rse.2008.01.022>
- Hill MJ (2013) Vegetation index suites as indicators of vegetation state in grassland and savanna: an analysis with simulated SENTINEL 2 data for a North American transect. *Remote Sens Environ* 137:94–111
- Holbrook JE (1838) North American herpetology, vol 4. J. Dobson, Philadelphia
- Huang C, Asner GP (2009) Applications of remote sensing to alien invasive plant studies. *Sensors* 9:4869–4889. <https://doi.org/10.3390/s90604869>
- Huang H, Gong P, Clinton N, Hui F (2008) Reduction of atmospheric and topographic effect on Landsat TM data for forest classification. *Int J Remote Sens* 29:5623–5642
- Immitzer M, Vuolo F, Atzberger C (2016) First experience with Sentinel-2 data for crop and tree species classifications in central Europe. *Remote Sens* 8:166
- Knipling EB (1970) Physical and physiological basis for the reflectance of visible and near-infrared radiation from vegetation. *Remote Sens Environ* 1:155–159
- Laba M, Downs R, Smith S et al (2008) Mapping invasive wetland plants in the hudson river national estuarine research reserve using quickbird satellite imagery. *Remote Sens Environ* 112:286–300
- Lelong B, Lavoie C, Jodoin Y, Belzile F (2007) Expansion pathways of the exotic common reed (*Phragmites*

- australis*): a historical and genetic analysis. *Divers Distrib* 13:430–437
- Lopez RD, Edmonds CM, Neale AC, Slonecker T, Jones KB, Heggem DT, Lyon JG, Jaworski E, Garofalo D, Williams D (2004) Accuracy assessments of airborne hyper-spectral data for mapping opportunistic plant species in fresh-water coastal wetlands. In: Lunetta RS, Lyon JG (eds) *Remote sensing and GIS accuracy assessment*. CRC Press, New York, pp 253–267
- Lu D, Weng Q (2007) A survey of image classification methods and techniques for improving classification performance. *Int J Remote Sens* 28:823–870
- Lyon JG, McCarthy J (1995) *Wetland and environmental applications of GIS*. CRC Press, Boca Raton
- Mann DL, Nelson JG (1980) Ideology and wildlands management: the case of Rondeau Provincial Park, Ontario. *Environ Manag* 4:111–124
- Marcaccio JV, Chow-Fraser P (2016) Mapping options to track invasive *Phragmites australis* in the Great Lakes basin in Canada. Proceedings of 3<sup>rd</sup> International Conference “Water resources and wetlands”. Tulcea
- Marcaccio, Chow-Fraser P (2018) Mapping invasive *Phragmites australis* in highway corridors using provincial orthophoto databases in Ontario
- Marcaccio JV, Markle CE, Chow-Fraser P (2016) Use of fixed-wing and multi-rotor unmanned aerial vehicles to map dynamic changes in a freshwater marsh. *J Unmanned Veh Syst* 4:193–202
- Markle CE, Chow-Fraser P (2018) Effects of European common reed on Blanding’s turtle spatial ecology. *J Wildl Manag* 25:15. <https://doi.org/10.1002/jwmg.21435>
- Marks M, Lapin B, Randall J (1994) *Phragmites australis* (*P. communis*): threats, management and monitoring. *Nat Areas J* 14:285–294
- McLaughlin C (1993) *Ecosystem management in Rondeau Provincial Park*. Altern J 19:6
- McNabb CD, Batterson TR (1991) Occurrence of the common reed, *Phragmites australis*, along roadsides in Lower Michigan. *Alma, Mich Acad*
- Melgani F, Bruzzone L (2004) Classification of hyperspectral remote sensing images with support vector machines. *IEEE Trans Geosci Remote Sens* 42(8):1778–1790. <https://doi.org/10.1109/TGRS.2004.831865>
- Meloche C, Murphy SD (2006) Managing tree-of-heaven (*Ailanthus altissima*) in parks and protected areas: a case study of Rondeau Provincial Park (Ontario, Canada). *Environ Manag* 37:764–772. <https://doi.org/10.1007/s00267-003-0151-x>
- Mestre H (1935) The absorption of radiation by leaves and algae. *Cold Spring Harb Symp Quant Biol* 3:191–209. <https://doi.org/10.1101/SQB.1935.003.01.023>
- Meyerson LA, Saltonstall K, Windham L et al (2000) A comparison of *Phragmites australis* in freshwater and brackish marsh environments in North America. *Wetl Ecol Manag* 8:89–103
- Morel A, Bélanger S (2006) Improved detection of turbid waters from ocean color sensors information. *Remote Sens Environ* 102:237–249
- Mountrakis G, Im J, Ogole C (2011) Support vector machines in remote sensing: a review. *ISPRS J Photogramm Remote Sens* 66:247–259. <https://doi.org/10.1016/j.isprsjprs.2010.11.001>
- Oetter DR, Cohen WB, Berterretche M et al (2001) Land cover mapping in an agricultural setting using multiseasonal Thematic Mapper data. *Remote Sens Environ* 76:139–155
- Ozesmi SL, Bauer ME (2002) Satellite remote sensing of wetlands. *Wetl Ecol Manag* 10:381–402
- Pal M, Mather PM (2005) Support vector machines for classification in remote sensing. *Int J Remote Sens* 26(5):1007–1011
- Peterson EB (2005) Estimating cover of an invasive grass (*Bromus tectorum*) using tobit regression and phenology derived from two dates of Landsat ETM+ data. *Int J Remote Sens* 26:2491–2507. <https://doi.org/10.1080/01431160500127815>
- Rasolofoharino M, Blasco F, Bellan MF, Aizpuru M, Gauquelin T, Denis J (1998) A remote sensing based methodology for mangrove studies in Madagascar. *Int J Remote Sens* 19(10):1873–1886
- Resasco J, Hale AN, Henry MC, Gorchov DL (2007) Detecting an invasive shrub in a deciduous forest understory using late-fall Landsat sensor imagery. *Int J Remote Sens* 28:3739–3745
- Rickey MA, Anderson RC (2004) Effects of nitrogen addition on the invasive grass *Phragmites australis* and a native competitor *Spartina pectinata*. *J Appl Ecol* 41:888–896
- Rupasinghe PA, Simic Milas A, Arend K, Simonson MA, Mayer C, Mackey S (2018) Classification of shoreline vegetation in the Western Basin of Lake Erie using airborne hyperspectral imager HSI2, Pleiades and UAV data. *Int J Remote Sens* 40:3008
- Saltonstall K (2002) Cryptic invasion by a non-native genotype of the common reed, *Phragmites australis*, into North America. *Proc Natl Acad Sci* 99:2445–2449
- Schmidt KS, Skidmore AK (2001) Exploring spectral discrimination of grass species in African rangelands. *Int J Remote Sens* 22:3421–3434
- Sinclair TR, Schreiber MM, Hoffer RM (1968) Pathway of solar radiation through leaves I. *Agron J* 65(2):276–283
- Sohn Y, McCoy RM (1997) Mapping desert shrub rangeland using spectral unmixing and modeling spectral mixtures with TM data. *Photogramm Eng Remote Sens* 63:707–716
- Stratoulas D, Balzter H, Sykioti O et al (2015) Evaluating sentinel-2 for lakeshore habitat mapping based on airborne hyperspectral data. *Sensors* 15:22956–22969
- Tottrup C (2004) Improving tropical forest mapping using multi-date Landsat TM data and pre-classification image smoothing. *Int J Remote Sens* 25:717–730
- Tuanmu M-N, Viña A, Bearer S et al (2010) Mapping understory vegetation using phenological characteristics derived from remotely sensed data. *Remote Sens Environ* 114:1833–1844
- Tulbure MG, Johnston CA, Auger DL (2007) Rapid invasion of a Great Lakes coastal wetland by non-native *Phragmites australis* and Typha. *J Gt Lakes Res* 33:269–279
- Uddin M, Robinson RW, Caridi D et al (2014) Suppression of native *Melaleuca ericifolia* by the invasive *Phragmites australis* through allelopathic root exudates. *Am J Bot* 101:479–487
- Vapnik VN, Kotz S (1982) *Estimation of dependences based on empirical data*. Springer, New York

- Wilcox DA (2012) Response of wetland vegetation to the post-1986 decrease in Lake St. Clair water levels: seed-bank emergence and beginnings of the *Phragmites australis* invasion. *J Gt Lakes Res* 38:270–277
- Wilcox I (n.d.) Wetland Meadow Marsh Community - surface area, supply-based (Lake Ontario & Thousand Islands). [http://www.losl.org/twg/pi/pi\\_meadowmarsh-e.html](http://www.losl.org/twg/pi/pi_meadowmarsh-e.html). Accessed 17 May 2018
- Wilcox KL, Petrie SA, Maynard LA, Meyer SW (2003) Historical distribution and abundance of *Phragmites australis* at long point, Lake Erie, Ontario. *J Gt Lakes Res* 29:664–680
- Williams AP, Hunt ER Jr (2002) Estimation of leafy spurge cover from hyperspectral imagery using mixture tuned matched filtering. *Remote Sens Environ* 82:446–456
- Wilstxter R, Stoll A (1918) Untersuchungen fiber die Assimilation der Kohlensäure. Julius Springer Berl 344
- Young BE, Young G, Hogg AR (2011) Using Landsat TM NDVI change detection to identify *Phragmites* infestation in southern Ontario coastal wetlands. *Ont. Min. Nat. Resour., Inventory Monitoring and Assessment*, Peterborough: 32
- Zhang X, Friedl MA, Schaaf CB et al (2003) Monitoring vegetation phenology using MODIS. *Remote Sens Environ* 84:471–475
- Zhang C, Xie Z (2013) Object-based vegetation mapping in the Kissingmee River watershed using HyMap data and machine learning techniques. *Wetlands* 33(2):233–244. <https://doi.org/10.1007/s13157-012-0373-x>
- Zheng B, Myint SW, Thenkabail PS, Aggarwal RM (2015) A support vector machine to identify irrigated crop types using time-series Landsat NDVI data. *Int J Appl Earth Obs Geoinform* 34:103–112. <https://doi.org/10.1016/j.jag.2014.07.002>

**Publisher's Note** Springer Nature remains neutral with regard to jurisdictional claims in published maps and institutional affiliations.